Heat Transport by Planetary Waves in a Nonlinear Quasi-geostrophic Model

 by Yibing Chen

A thesis submitted to the Faculty of Graduate Studies and Research in partial fulfillment of the requirements for the degree of Master of Science.

February, 1989

Department of Meteorology

McGill University

Montreal, Quebec, Canada

Heat Transport by Planetary Waves in a Nonlinear Quasi-geostrophic Model

ABSTRACT

We examine the zonal and meridional heat transport of planetary waves in a 10-level, nonlinear, quasi-geostrophic, mid-latitude β-plane channel model. Large scale surface topography acts as the zonally asymmetric forcing; while forcing of the mean zonal wind is relaxation to a climatological distribution. Eddy statistics based on the last 30 days of two 160-day simulations are calculated. There is no topography in the first simulation, while topography is present in the second experiment.

The presence of surface topography shifts the zonal wavenumber maximum of the meridional eddy heat flux from the synoptic scales to the larger planetary scales, in agreement with results from linear models. The results also demonstrate the dissipative role of transient eddies on the zonally asymmetric component of the time mean temperature field, as found in observational studies. This is accomplished by the zonal and meridional heat fluxes directed down the local temperature gradient. The corresponding energy conversion from stationary eddy to transient eddy available potential energy in the model is also examined.

Résumé

Nous examinons le transport de chaleur méridional et zonal des ondes planétaires avec un modèle de canal, à 10 niveaux, non-linéaire, quasi-géostrophique, de latitudes moyennes et dans le plan-β. La topographie de surface à grande échelle agit comme contrainte assymétrique zonale alors que celle sur le vent zonal moyen est la relaxation de la distribution climatologique.

Des statistiques sur les tourbillons, basées sur les derniers 30 jours de deux simulations de 160 jours, sont calculées. Il n' y a pas de topographie dans la première simulation, mais elle est présente dans la deuxième expérience.

La présence de la topographie de surface déplace le maximum du nombre d'onde zonal du flux de chaleur tourbillonnaire méridional, des échelles synoptiques vers des échelles plus larges, ce qui est en accord avec les résultats des modèles linéaires. Les resultats démontrent également le rôle dissipatif des tourbillons transitoires sur la composante assymétrique zonale du champ de température moyen (moyenne temporelle), tel que démontré dans les études d'observations. Ceci est accompli lorsque les flux de chaleur zonaux et méridionaux sont dirigés vers le gradient local de température. L'énergie de conversion correspondante, du tourbillon stationnaire au tourbillon transitoire d'énergie potentielle disponible dans le modèle, est aussi examinée.

Acknowledgements

I wish to avail myself of this opportunity to extend to my supervisor, Professor C.A. Lin, my heartfelt thanks for his invaluable guidance.

Furthemore I am grateful to Dr. Herschel L. Mitchell for his computer code, which served as a prototype for the model used in this study.

I acknowledge with thanks the financial support provided by the Natural Sciences and Engineering Research Council, and the Atmospheric Environment Service.

I would also like to thank Ms. Ursula Seidenfuss who drafted many of the figures in this thesis and Mr. Alan Schwartz for his support in solving computing problems.

Last but not least, I would like to thank the Department of Meteorology at McGill University for the assistance which I received throughout my studies.

TABLE OF CONTENTS

List of Figures

CHAPTER 1

Introduction

Planetary waves are a significant component of the mid-latitude atmospheric general circulation. They play a crucial role in maintaining the balance of heat, momentum and water vapour in the atmosphere, through their various eddy transports. In order to better understand the nature of these eddies, the wind and temperature fields are often decomposed into the mean, stationary and transient components. The time and zonal average of the meridional heat transport can be written in the form

$$[\overline{VT}] = [\bar{V}][\bar{T}] + [\bar{V}^*\bar{T}^*] + [\overline{V'T'}] \qquad (1.1)$$

where V and T denote meridional velocity and temperature, brackets and overbars denote zonal and time means, and asterisks and primes denote departures from zonal and time means respectively. The terms on the right hand side of (1.1) are refered to as the zonal mean (Z) component, the stationary eddy (SE) component and the transient eddy (TE) component respectively. In addition to occuring on different time scales, atmospheric eddies also cover a wide range of space scales. Planetary scale TE's and SE's are highly baroclinic and account for a substantial portion of the total eddy heat transport. Figure 1.1, from Kao and Sagendorf (1970), shows the zonal wavenumber spectra of the meridional heat transport by SE's and TE's at 850mb, 60^{o}N in winter. Both spectra peak at wavenumber 3. In this thesis, we are concerned primarily with both the zonal and meridional heat transports of planetary waves.

Stone (1977) suggested that planetary scale TE's and baroclinic SE's

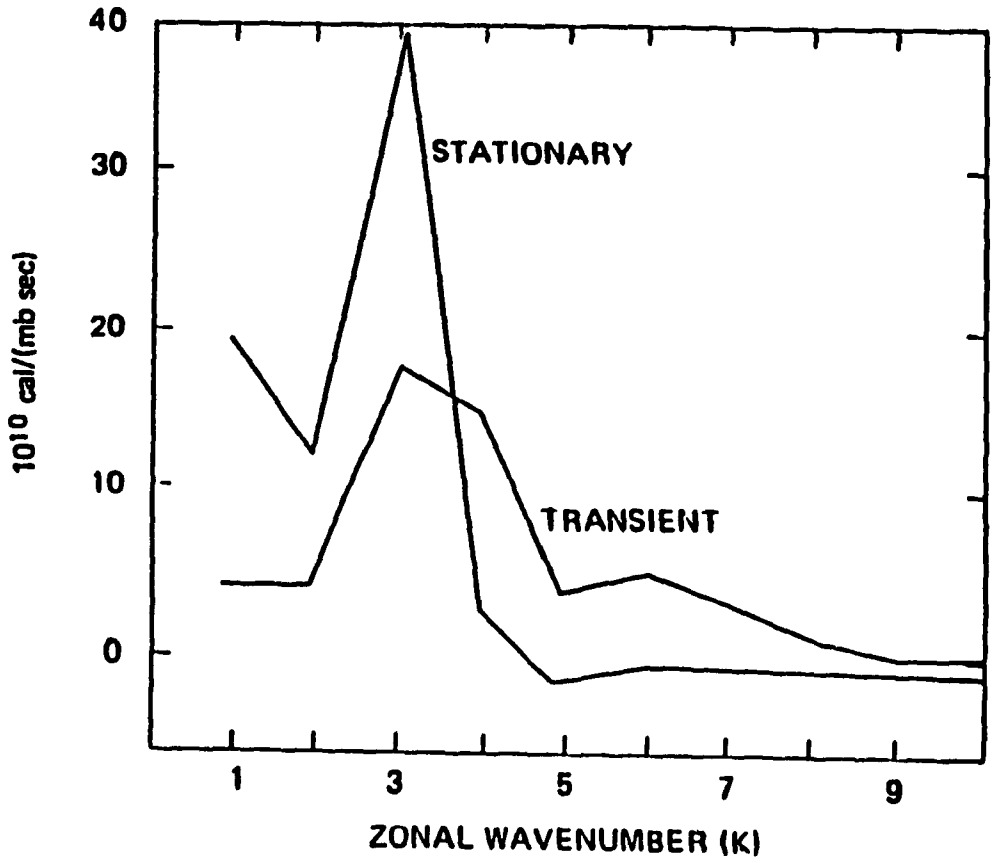

Figure 1.1 Observed wavenumber spectra of meridional sensible heat transport by stationary and transient eddies at 850mb, 60°N in winter (from Kao and Sagendorf, 1970)

might merely be two different aspects of a single phenomenon - eddies generated by a cooperation between forcing and baroclinic instability. Such eddies would be baroclinic in nature and planetary scale in size, and could contain both TE and SE components. Lin (1980 a, b) examined this hypothesis by investigating the stability properties of a basic state consisting of long wave superposed on a baroclinic zonal flow. The eddy heat flux spectrum of the most unstable mode peaked in the planetary scales, in agreement with observations. The zonal scale selection mechanism was decribed in terms of the energy release associated with the baroclinic instability of the wavy basic state. Frederiksen (1978) found that the growth rates of unstable modes are increased by superposing a baroclinic long wave upon a zonal mean flow. Regions of maximum mode growth were related to the baroclinicity of the basic flow. The stability criterion was later generalized to include the basic flow horizontal shear (Frederiksen, 1980). Sasamori and Youngblut (1981) also showed that planetary, zonally asymmetric forcing can provide for transient waves, through the instability of a prescribed stationary wave to perturbations of highly restricted form. In more recent works, Frederiksen (1982, 1983a, 1983b) used realistic basic states derived from Northern Hemisphere climatology. A variety of unstable modes was obtained, including propagating monopole cyclogenesis modes, onset - of - blocking modes, and low frequency teleconnection modes. Simmons et al (1983) also obtained teleconnection modes using a global barotropic model, linearized about the mean January flow. Neelin and Lin (1984) examined the baroclinic instability of forced stationary waves and found that one of the dominant modes is quasi-stationary and resembled the observed stationary wave

pattern. Grotjahn (1984) has provided a review of studies of instability of zonally asymmetric flows.

The result that baroclinic instability in the presence of zonally asymmetric forcing can generate transient planetary waves is also supported by observational studies (Lau, 1979; Lau and Wallace, 1979; Lau and Oort, 1982; Boer and Sargent, 1985). These studies show that the transient eddy heat flux is directed down the local temperature gradient of the time mean temperature field. Thus the eddy heat transports act to destroy the departures from zonal asymmetry of the temperature field. Lau (1979) estimated a time scale of several days associated with this dissipative effect of the transients on the zonally asymmetric conponent of the mean temperature field.

In this thesis, we use a multi-level nonlinear quasi-geostrophic β-planc model to examine the role of asymmetric forcing in the form of surface topography, in the heat transport of transient and stationary plantary waves. The high vertical resolution is needed because the instability of zonally asymmetric states can give rise to unstable modes of very different vertical scales (Lin, 1987): modes characterizing low-frequency variability are deep and extend through the troposphere, wheras modes associated with localized cyclogenesis tend to be much shallower. These different modes would not be adequately resolved with a 2-level model. The nonlinearity is also expected to be important as it provides a nonlinear wave-wave coupling between the transient and stationary waves. This coupling is crucial to the dissipative effect of the transient eddy heat transport discussed earlier.

The next chapter provides a description of the model and of the

model parameters. Chapter 3 presents the results on the meridional heat transport by the model planetary waves, while Chapter 4 discusses the zonal heat transports. The final chapter contains the conclusions.

CHAPTER 2

A Nonlinear, β-plane, Quasi-Geostrophic Numerical Model

2.1. Governing equations

The numerical model that we use to examine planetary wave heat transport is a nonlinear, mid-latitude β-plane quasi-geostrophic model, with a spectral formulation in the horizontal, and finite differencing in the vertical. The model was first formulated by Mitchell (1982) to examine the resonance of stationary waves in the troposphere and stratosphere (Mitchell and Derome, 1983; 1985). The model equatios, with a forcing term present in the geostrophic vorticity equation, may be written as follows.

$$\frac{\partial}{\partial t}\nabla^2\Psi + J(\Psi\ ,\ \nabla^2\Psi + f) - f_o \frac{\partial \omega}{\partial p} = F \qquad (2.1)$$

$$\frac{\partial}{\partial t}(\frac{\partial \Psi}{\partial p}) + J(\Psi,\frac{\partial \Psi}{\partial p}) + \frac{\sigma}{f_o}\omega = 0 \qquad (2.2)$$

Here J is the horizontal Jacobian in the zonal (x) and meridional (y) directions; it represents the advection terms. The horizontal Laplacian is denoted ∇^2. The Coriolis parameter is $f=f_o+\beta y$, with f_o being the value at 45^oN, and β its meridional gradient at the same latitude; this is the mid-latitude β-plane approximation. The symbols t, p, ω, σ denote time, pressure, vertical pressure velocity (ω=dp/dt), and static stability parameter $\sigma = -\frac{\alpha}{\theta}\frac{\partial \theta}{\partial p}$ respectively, with α being the specific volume and θ the potential temperature.

The forcing F in (2.1) operates only in the time mean zonal flow ($\bar{U}$),

with corresponding streamfunction ($\bar{\Psi}$). It forces the mean flow to some specified state ($\bar{U}^*$, $\bar{\Psi}^*$), and represents the forcing of a baroclinic mean flow by the radiation field. The detailed manner in which the zonal circulation is maintained is not our concern here, and its overall effect is included by defining

$$F = \bar{F} = h_0\left(\frac{\partial \bar{U}}{\partial y} - \frac{\partial \bar{U}^*}{\partial y} \right) = -h_0\left(\nabla^2\bar{\Psi} - \nabla^2\bar{\Psi}^* \right) \qquad (2.3)$$

where the coefficient h_0 is inversely proportional to the relaxation time scale of the zonal forcing. The other external forcing in the model is by surface topography, which is represented as a vertical velocity forced at the lower boundary. This is discussed later in the formulation of the model boundary conditions. Eq (2.1) thus represents the geostrophic vorticity equation with a zonal forcing, while (2.2) is the adiabatic temperature equation.

The model atmosphere is in a β-plane channel with rigid walls at the southern (y=0) and northern (y=D) boundaries. The model is periodic in the zonal direction, and extends from x=0 to x=L. The distances D and L are associated with the equator-to-pole distance, and the circumference of the latitude circle at 45°N respectively. The β-plane approximation is strictly not valid over such a larger latitudinal extent, but the quasi-geostrophic system on a β-plane is often used beyond its strict range of validity to examine planetary scale phenomena. Despite its relative simplicity compared to spherical geometry, the results so obtained are generally qualitatively correct. This can be expected to be the case in the present situation, where we focus on the interaction between planetary TE's and SE's via their heat transports.

The boundary condition at the channel walls is the vanishing of the

normal velocity

$$v = \frac{\partial \Psi}{\partial x} = 0 \qquad \text{at} \quad y=0,\ D \tag{2.4}$$

At the top of the model atmosphere, the vertical pressure velocity is required to vanish,

$$\omega = 0 \qquad \text{at} \quad p=0 \tag{2.5}$$

The use of this top boundary condition is equivalent to applying a rigid lid at some finite presure which is dependent on the vertical resolution of the model (Lindzen et al., 1968; Nakamura, 1976; Kirkwood and Derome, 1977). This means that spurious reflection of wave energy could take place. For the most part of this study, we examine eddy statistics which have their maximum value away from the top boundary, thus minimizing this spurious effect.

We consider the bottom of the model domain to correspond to the top of the planetary boundary layer. Both surface topography and surface drag induce vertical motion at the bottom of the free atmosphere. These effects are incorporated by the following Ekman pumping parameterization.

$$\omega_B = \rho f_0 \frac{\partial \Psi_B}{\partial t} - \rho g \left[J(\Psi_B, H_T) + \left(\frac{K}{2f_o}\right)^{1/2} \nabla^2 \Psi_B \right] \tag{2.6}$$

The subscript B denotes values at the bottom of the model domain; ρ, g, H_T, K are the density, gravitational acceleration, topographic height and eddy viscosity respectively.

2.2 Model discretization

The model equations are discretized in the vertical, using N=10 levels. Pressure is used as the vertical coordinate, with the model atmosphere divided into 10 layers. The pressure increment between the

levels is thus 100mb, with p_s=1000mb being the mean surface pressure. A schematic representation of the vertical discretization is shown in Fig. 2.1. The dependent variables as given in (2.1) and (2.2) are the streamfunction (Ψ_i: i=1,3,.....,2N-1) and the pressure vertical velocity (ω_i: i=0,2,.....,2N), with the subscript i denoting level number. The top boundary condition (2.5) is ω_o=0, and the bottom boundary condition (2.6) is $\omega_{2N} = \omega_B$. The governing vorticity (2.1) and temperature (2.2) equations are written at odd and even levels respectively. Following Lorenz (1963) we choose a set of orthogonal basis functions to represant the zonal and meridional variations:

$$\Phi_{on}=\sqrt{2}\cos\frac{\pi}{D}ny$$

$$\Phi_{mn}= 2\cos\frac{2\pi}{L}mx\ \sin\frac{\pi}{D}ny \qquad (2.7)$$

$$\Phi'_{mn}= 2\sin\frac{2\pi}{L}mx\ \sin\frac{\pi}{L}ny$$

where m, n are integers representing the zonal and meridional wavenumbers respectively. The above basis functions are eigenfunctions of the Laplacian operator, satisfy an orthogonality condition, and have vanishing tangential derivatives at the channel walls.. The latter property means that the meridional boundary condition (2.4) is automatically satisfied with these basis functions. The Jacobian of two orthogonal functions can be expressed as a series involving the complete set of functions. Thses properties are discussed in detail in Lorenz (1963) and Mitchell (1982).

The dependent variables (Ψ_i, ω_i) at each level are expanded using the set of basis functions (2.7), resulting in a set of time-dependent spectral amplitude coefficients. The details of the truncation of this expansion will be discussed in the next section. The set of governing equations

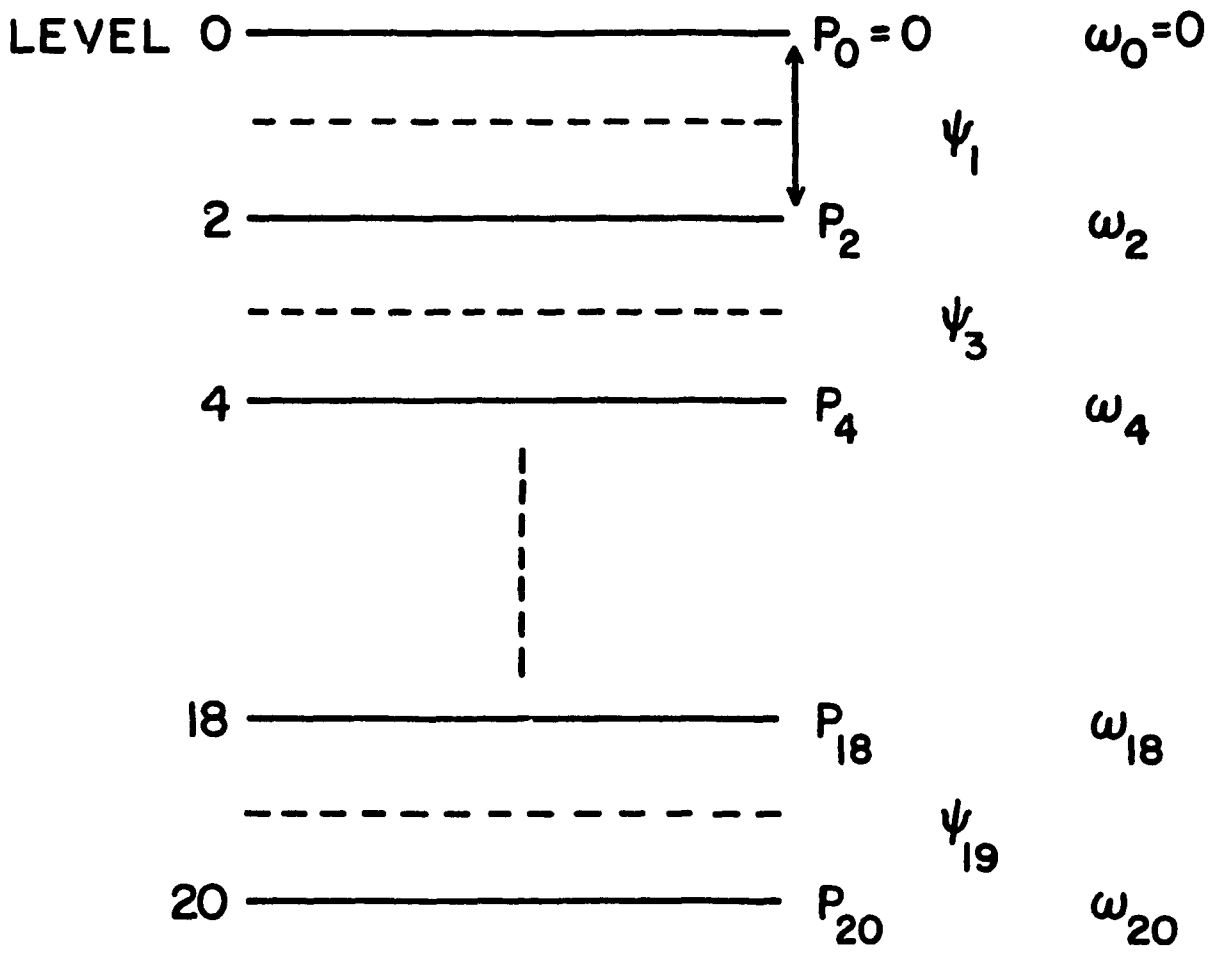

Figure 2.1 Vertical discretization of the model: p_k, Ψ_k, ω_k denote the pressure, streamfunction and pressure vertical velocity at level k.

(2.1), (2.2) then reduces to a set of coupled nonlinear ordinary differential equations for the time tendencies of the spectral coefficients. These equations are integrated using a time marching procedure. Centered time differences are used for all timesteps except for the initial step, where forward differences are applied. All terms are evaluated at the current time step, except for the surface drag and zonal flow driving terms, which are lagged one time step to maintain numerical stability (Haltiner and Williams, 1980). A weak time filter (Robert, 1966; Asselin, 1972) is used to suppress the spurious growth of the computational mode. We note that a number of tests were carried out by Mitchell (1982) to verify the model formulation and the corresponding computer code.

2.3 Specification of model parameters

As discussed in section 2.1, the zonal (L) and meridional (D) extents of the model domain are taken to be the circumference of the latitude circle at latitude ϕ_o=45°N, and the equator - to - pole distance respectively.

$$L = 2\pi a \cos\phi_o$$

$$D = \frac{1}{2}\pi a$$

Here, a is the radius of the earth. The horizontal resolution is described by five even zonal wavenumbers (m=2, 4, 6, 8, 10), and ten meridional wavenumbers (n=1, 2, ..., 10). This choice of the wavenumber truncation resolves the radius of deformation, which characterizes the zonal scale of a baroclinically unstable mode. The use of only even zonal wavenumbers reduces the computational requirements considerably. A full spectrum of meridional modes means that significant nonlinear interaction may take place. We note that O'Brien and Branscome (1988) concluded that a minimum

truncation of a quasi-geostrophic 2-level model needed to adequately represent the gross features of the general circulation is 3 zonal modes and 3 meridional modes. Our principal aim here is somewhat different: to examine the mechanistic role of surface topography in the interaction between stationary and transient planetay waves.

In the vertical, N=10 levels are used with a mean surface pressure of p_s=1000mb. The pressure increment between levels is thus Δp=100mb. A time step of Δt=3600s is used; this is found to give stable results.

We assume, for simplicity, an isothermal vertical profile of the horizontally averaged temperature $\bar{T}$=239°K. This means that the static stability is a simple function of pressure

$$\sigma = \frac{R^2 T}{C_p p^2}$$

where C_p, R are the specific heat at constant pressure and the ideal gas constant respectively.

We perform two sets of experiments, one with the presence of surface topography and one without its presence. The topographic height H_T is of large horizontal scale, charactrized by zonal wavenumber m=2, and meridional wavenumber n=1,

$$H_T = A \sin \frac{2\pi}{L} 2x \sin \frac{\pi}{D} y$$

with the height amplitude being A=1000m.

The zonal flow driving $\bar{U}^*$ given in eq. (2.3) is taken to be the observed winter zonally averaged zonal flow from Oort and Rasmussen (1971). The latitude - pressure structure of the latter is shown in Fig. 2.2. This flow is in thermal wind balance with the meridional temperature gradient. It is baroclinically unstable, and its use as the zonal flow forcing gives

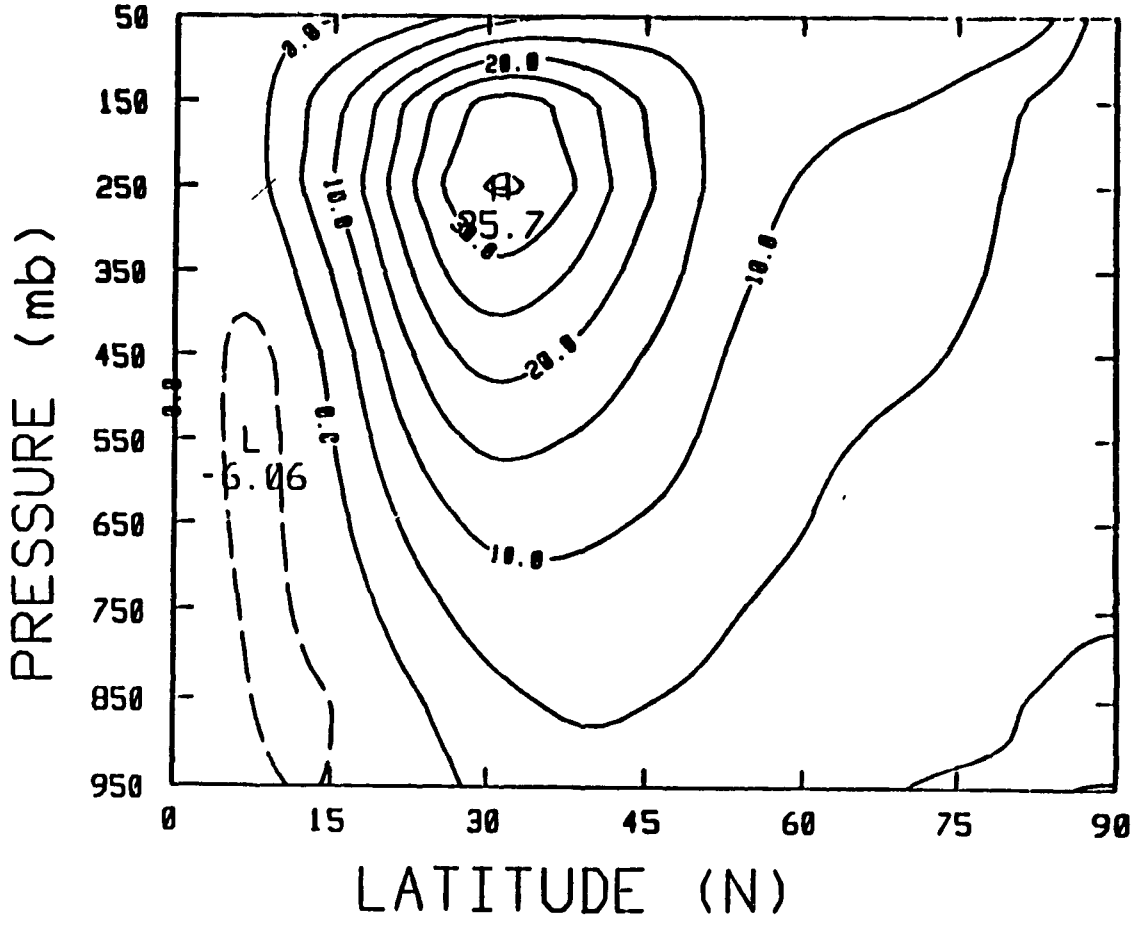

Figure 2.2 The latitude-pressure structure of the observed winter zonally averaged zonal flow [$\bar{U}$]. The contour interval is 5 m/s. (Adapted from Oort and Rasmusson, 1971).

rise to baroclinic eddies in the model. These eddies transport heat northward, acting to reduce the meridional temperature gradient. This in turn leads to a model generated zonal flow of weaker intensity and baroclinicity than the observed flow $\bar{U}^*$. Our goal is not to simulate the observed zonal wind, but rather to examine the heat transports of stationary and transient baroclinic planetary waves. The time scale of the zonal flow forcing in eq. (2.3) is given by $h_o=0.9\times10^{-6}s^{-1}$, corresponding to a relaxation time scale of about 13 days. The eddy viscosity characterizing the Ekman pumping formulation in eq. (2.6) is taken to be $K=5m^2/s$. For a barotropic vortex of depth H=10km, this yieds a spin-down time of $H(2/f_oK)^{1/2}$ =8 days.

The initial conditions for the experiments consist of a zonal flow equal to the zonal flow forcing $\bar{U}^*$, and a small amplitude superposed perturbation in the zonal wavenumber m=2 and the gravest meridional mode n=1.

CHAPTER 3

Planetary Wave Meridional Heat Transport

3.1 Zonally averaged basic wind and temperature fields

As described in the previous section, two sets of numerical experiments are conducted in this study. They are both 160 simulated days' duration, one without surface topography, and the other with topography. We refer to these cases as the NM ("no mountain") and M ("mountain") experiments respectively. The total kinetic energy (TKE), eddy kinetic energy (EKE) and zonal kinetic energy (ZKE) in the model domain are shown as a function of time in both experiments in Fig 3.1. We see that the TKE stabilizes after about 70 days, which is several times the time scale of the zonal flow forcing, h_0^{-1} ~13 days. A major difference between the two cases is that EKE is about twice as large in the M experiment. This is due to the larger conversion of ZKE to EKE in the presence of the zonally asymmetric surface topography. The last 30 days of the 160 day simulations are used for a diagnostic analysis of the eddy heat transport statistics. Thus in subsequant results, the time average will refer to an average over the period from days 130 to 160.

The time and zonally averaged zonal wind $[\bar{U}]$ is shown as a function of latitude and pressure in Fig. 3.2. Both cases show a jet stream structure similar to the observed structure in the winter troposphere (Fig. 2.2), but with reduced amplitudes. Recall the latter is also used as the zonal flow forcing. The reduced baroclinicity in both cases is due to the meridional heat transport by baroclinic waves. Note that westerlies are

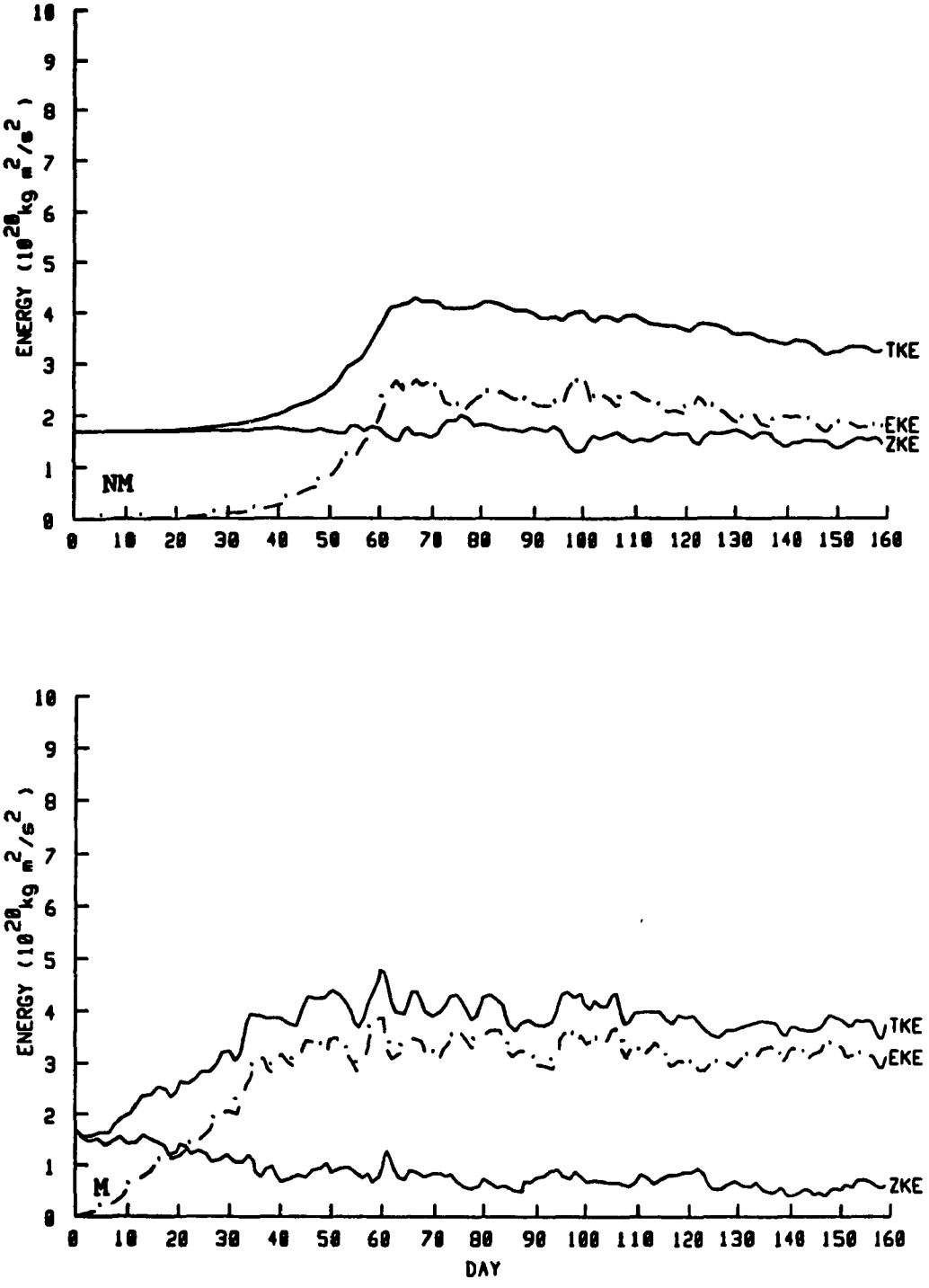

Figure 3.1 The model domain total kinetic energy (TKE), eddy kinetic energy (EKE) and zonal kinetic energy (ZKE) as a function of time, for the NM (no mountain; top) and M (mountain; bottom) experiments.

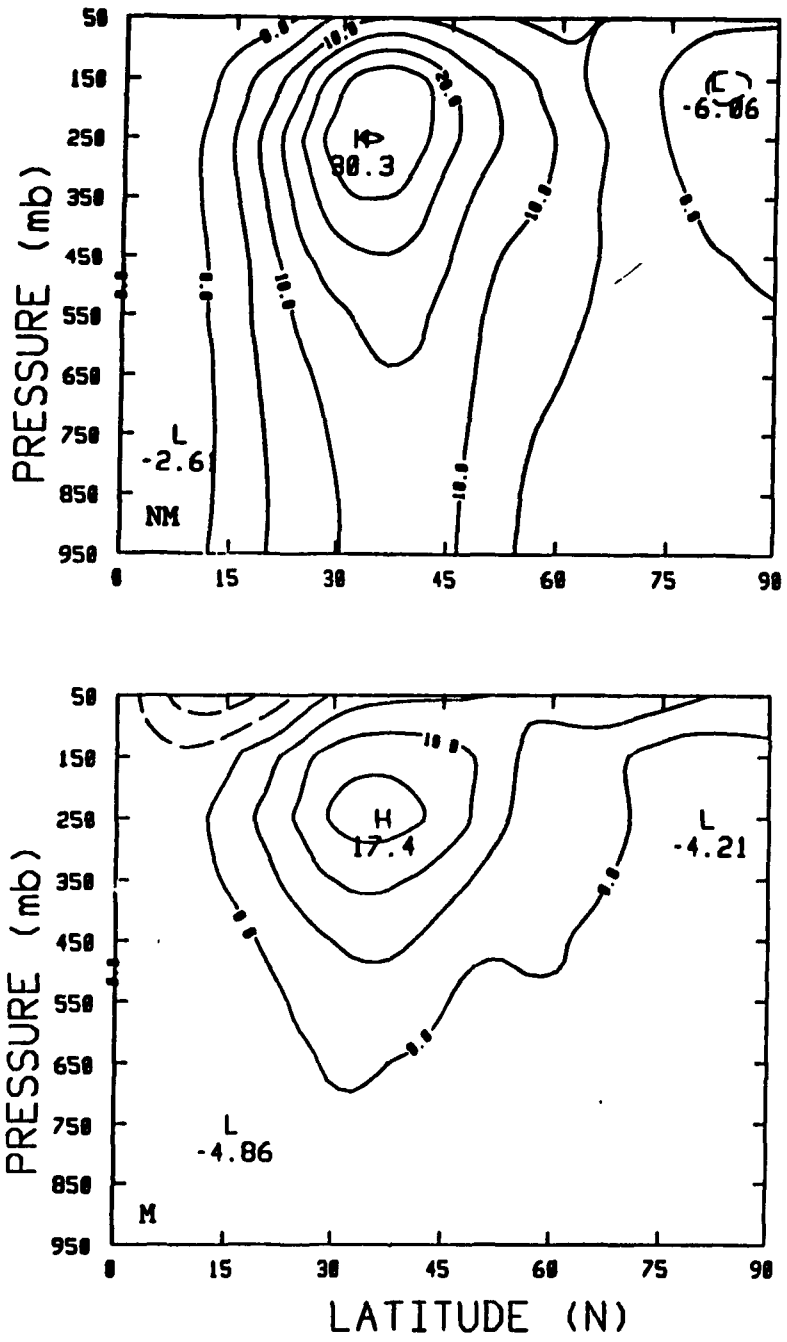

Figure 3.2 Meridional latitude-pressure section for the zonal and time averaged zonal wind field $[\bar{U}]$ for NM (up) and M (down) cases. The contour interval is 5 m/s.

found at low levels in the NM case, while easterlies are present near the surface in the M case. However, the baroclinicity is comparable for both cases, as the westerly jet is stronger in the NM case. The time and zonally averaged temperature fields $[\bar{T}]$, which is in thermal wind balance with the $[\bar{U}]$ field, are shown in Fig. 3.3. The two fields are comparable, with the maximum meridional temperature gradient in the mid-latitudes, where the maximum baroclinicity in the $[\bar{U}]$ field is located.

3.2 Stationary and transient eddy heat transports

The time and zonally averaged meridinal heat transport $[\overline{VT}]$ can be written as the sum of the transports by the zonal mean component $[\bar{V}][\bar{T}]$, the transient eddy (TE) component $[\overline{V'T'}]$ and the stationary eddy (SE) component $[\bar{V}^*\bar{T}^*]$.

$$[\overline{VT}] = [\bar{V}][\bar{T}] + [\overline{V'T'}] + [\bar{V}^*\bar{T}^*]$$

In our quasi-geostrophic model, the zonally averaged meridional velocity [V] vanishes, thus the zonally averaged meridional heat transport consists of only the TE and SE components. We show in Figs. 3.4 and 3.5 latitude-height sections of the total transport $[\overline{VT}]$, and the TE and SE components, for both the NM and M experiments respectively. In both cases, the total northward transport is maximum in the troposphere at about 30^{o}N; the maximum is located slightly higher at about 500mb in the NM case. The magnitude of the maximum is 4 times larger in the M case; a secondary maximum also occurs at about 300mb in this case. We note that such eddy maxima being located aloft is a characteristic of nonlinear models as well as of the observed circulation; maxima of eddy statistics from linear models are usually located at the surface (Green, 1970; Gall, 1976; Simmons

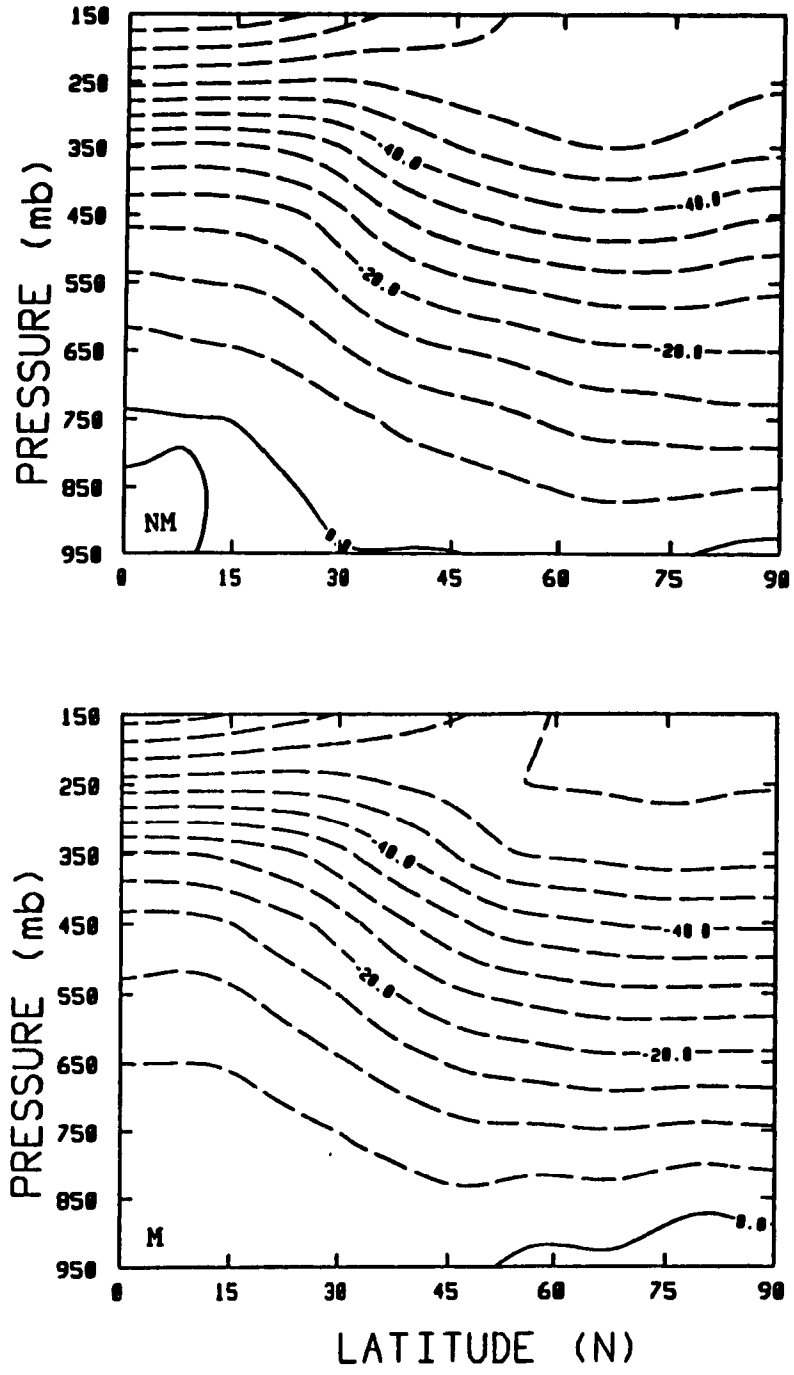

Figure 3.3 As Figure 3.2, but for the temperature field [$\bar{T}$]. The contour interval is 5 ^{o}C.

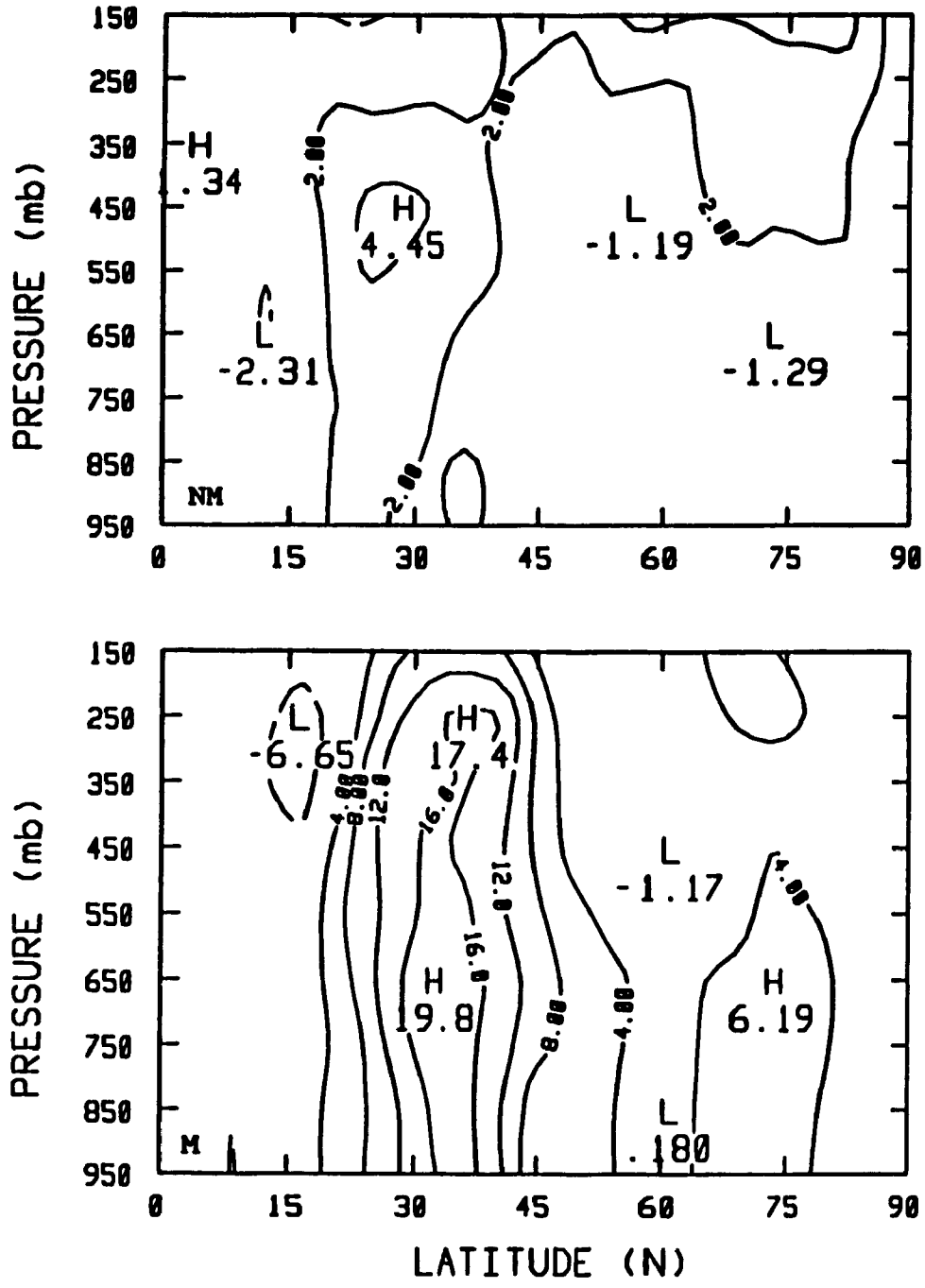

Figure 3.4 As Figure 3.2, but for the total zonal and time averaged meridional heat transport [$\overline{VT}$]. The contour interval is 2 °C m/s (up; NM) and 4 °C m/s (down; M), with the zero contour omitted.

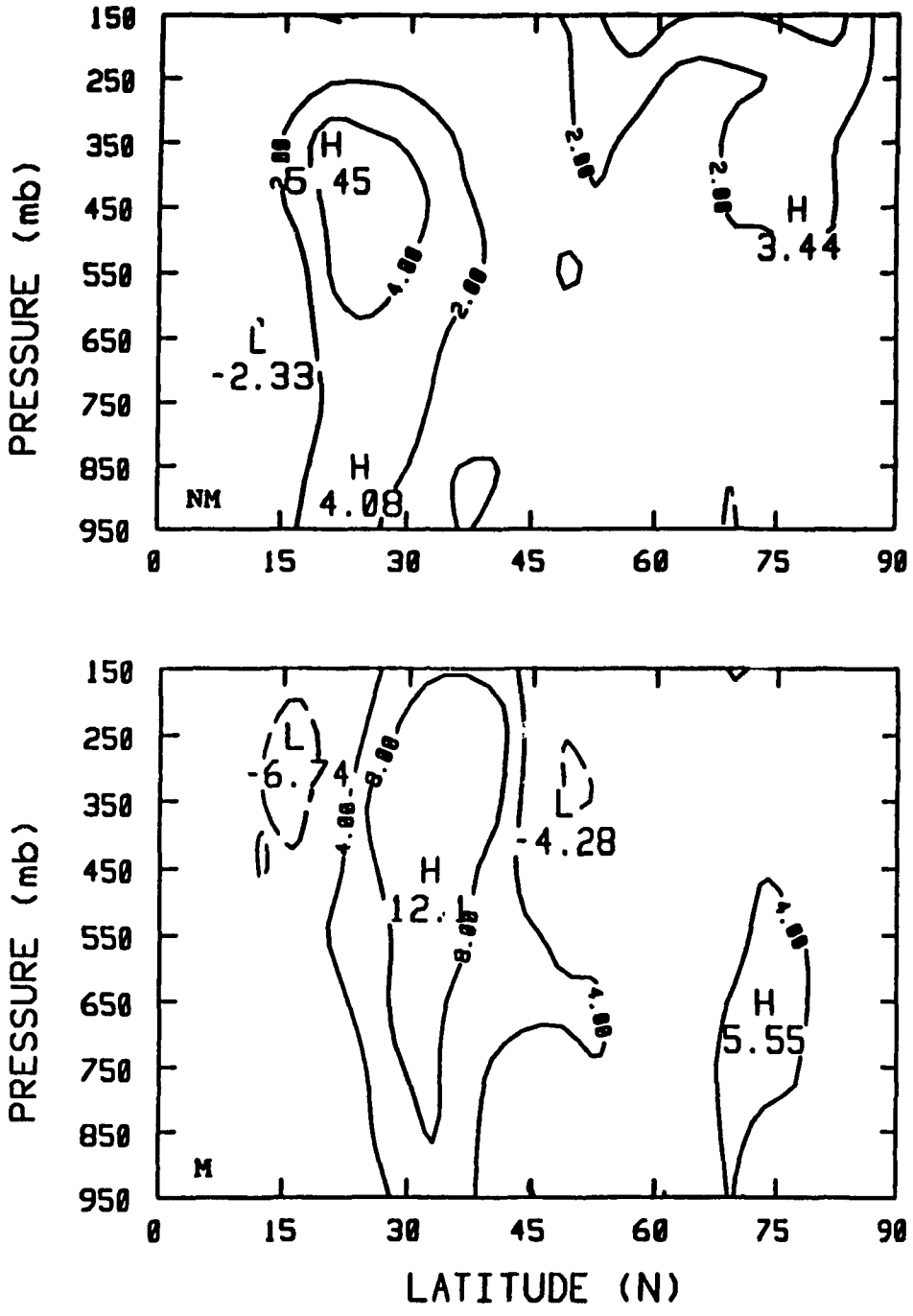

Figure 3.5a As Figure 3.2, but for TE component of the heat transport [$\overline{V'T'}$], with the zero contour omitted. The contour interval is 2 ^{o}C m/s (up; NM) and 4 ^{o}C m/s (down; M).

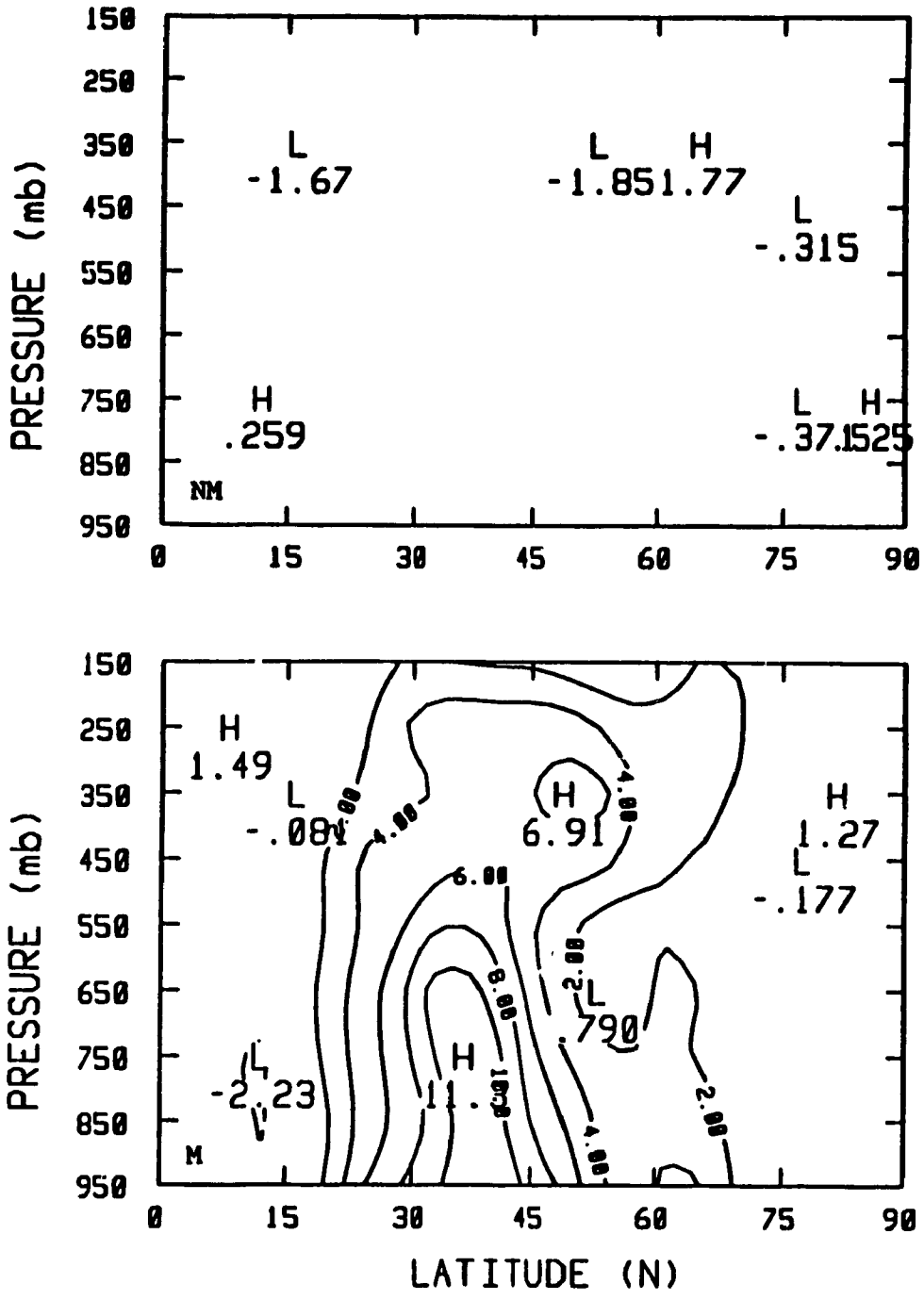

Figure 3.5b As Figure 3.2, but for SE component of the heat transport $[\bar{V}^*\bar{T}^*]$. The contour interval is 2 °C m/s for both MN (up) and M (down) cases, with the zero contour omitted.

and Hoskins, 1977; Frederiksen, 1981; Lin and Chan, 1988). The large increase in the total transport in the M case is due to increases in both the TE and SE components. The maximum aloft in the TE component is increased about threefold from the NM to the M case (Fig. 3.5a). The SE component in the NM case is weak and shows no organization (Fig. 3.5b). This is expected as the absence of surface topography means there is no zonal asymmetries to create favoured locations for SE development. In the M case, the SE component has an equivalent barotropic structure in the lower troposphere; its maximum is of comparable magnitude to that of the TE component. The significant enhancemant of the TE transport as well as the SE transport by surface topography suggests that there is significant nonlinear interaction between the TE's and SE's. Before examining further the nature of this interaction, we note that despite the large increase in the total meridional heat transport in the M case compared to the NM case, the temperature structure in the latitude-height plane remains relatively unchanged (Fig. 3.3). This is because the increased total transport in the M case is balanced by vertical advection. From the model temperature equation, we may derive the following time and zonally averaged equation.

$$\overline{\frac{\partial}{\partial t}\left[\frac{\partial \psi}{\partial p}\right]} - \frac{\partial}{\partial y}\left[\overline{\frac{\partial \psi}{\partial p}\frac{\partial \psi}{\partial x}}\right] + \frac{\sigma}{f_o}\left[\bar{\omega}\right] = 0$$

The tendency term is small when averaged over a 30-day period. The above then expresses a balance between meridional advection of temperature and vertical advection. In the M case, the vertical motion is significantly enhanced by the presence of surface topography. This allows for a larger meridional heat advection, leaving the temperature field largely unchanged.

We have noted earlier that the presence of topography leads to

significant wave-wave interaction in the M results. We now examine further the nature of this interaction. The zonally averaged meridional heat transport can be expressed as the sum of individual contributions from each zonal wavenumber (m=2, 4, 6, 8, 10). This can be done for both the TE and SE components. Physically, this decomposition expresses the fact that zonal wavenumber m in the perturbation streamfunction can interact with itself to provide a contribution to the zonally averaged TE and SE meridional heat transports. This contribution of each zonal wavenumber are now displayed as latitude-pressure sections, for both TE and SE components. Figure 3.6 shows the contributions of zonal wavenumbers m=6, 8 to the TE component for the NM case; Figures 3.7 and 3.8 show respectively the m=4, 6 contributions to the TE component, and the m=2, 4 contributions to the SE component for the M case. The latitude-pressure sections shown in Figures 3.6-3.8 correspond to the only zonal wavenumbers which show an organized structure on the meridional plane; they are also the ones with the largest amplitudes. The SE tranport in the NM case is weak for all zonal wavenumbers, and shows no structure. This is not surprising because the absence of zonal asymmetries means there are no favoured location for SE development, as discussed earlier. Thus in the NM case, most of the heat transport is accomplished by TE's of zonal wavenumbers m=6, 8. This zonal scale corresponds to the wavelength of maximum instability of a baroclinic zonal flow. In the M case, the increased heat transport noted earlier due to the presence of topography is realized through the planetary scales: m=4, 6 for TE's, and m=2, 4 for SE's as shown in Figure 3.7 and 3.8. Contributions from other zonal wavenumbers are small and show no organized latitude-pressure structure. The TE heat transport is maximum in the upper

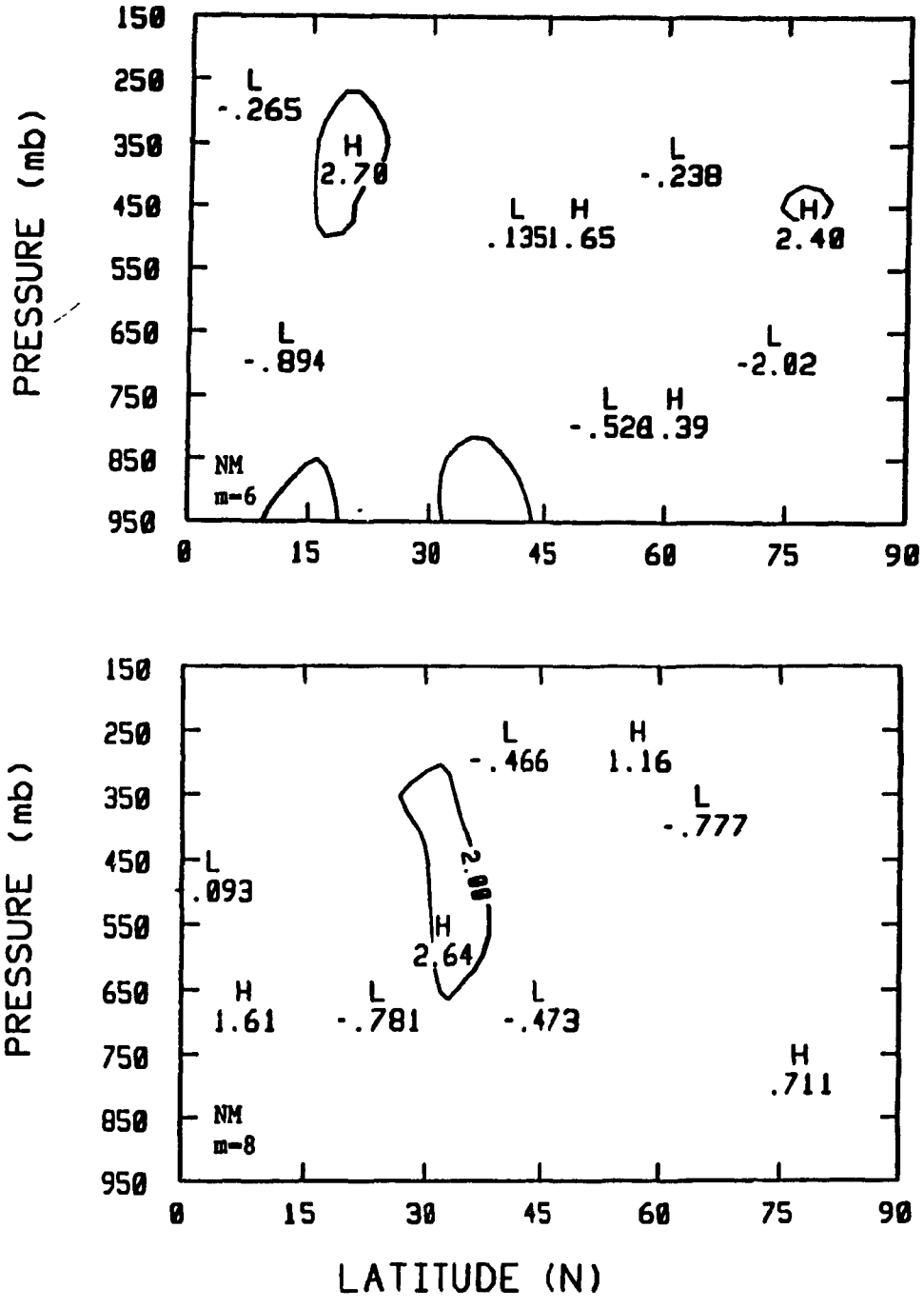

Figure 3.6 Meridional latitude-presure section for the contributions of zonal wavenumbers m=6 (up) and m=8 (down) to TE component $[\overline{V'T'}]$ for NM case. The contour interval is 2 ^{o}C m/s, with the zero contour omitted.

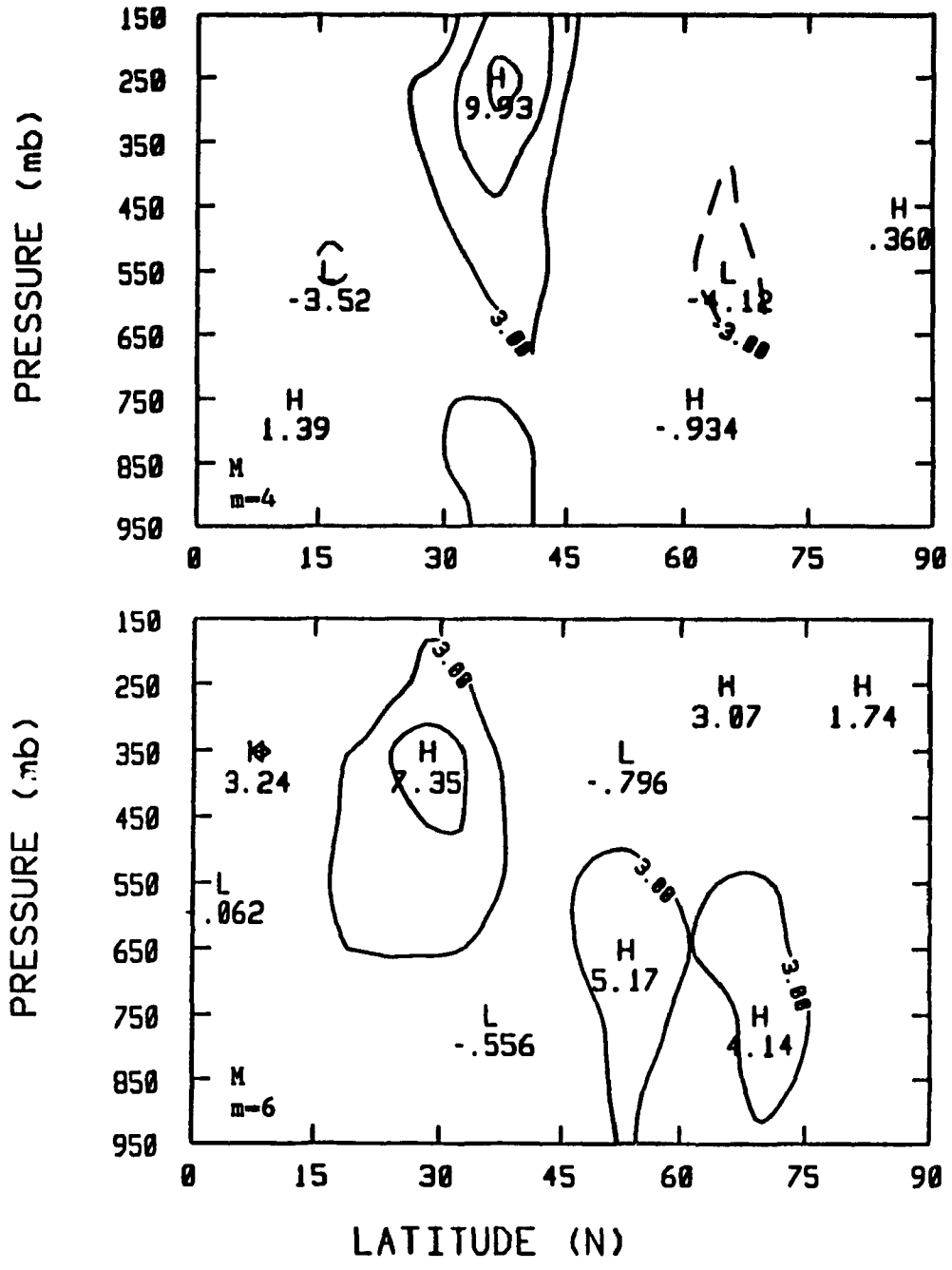

Figure 3.7 As Figure 3.6, but for the contributions of zonal wavenumbers m=4 (up) and m=6 (down) to TE component $[\overline{V'T'}]$ for M case. The contour interval is 3 ^{o}C m/s, with the zero contour omitted.

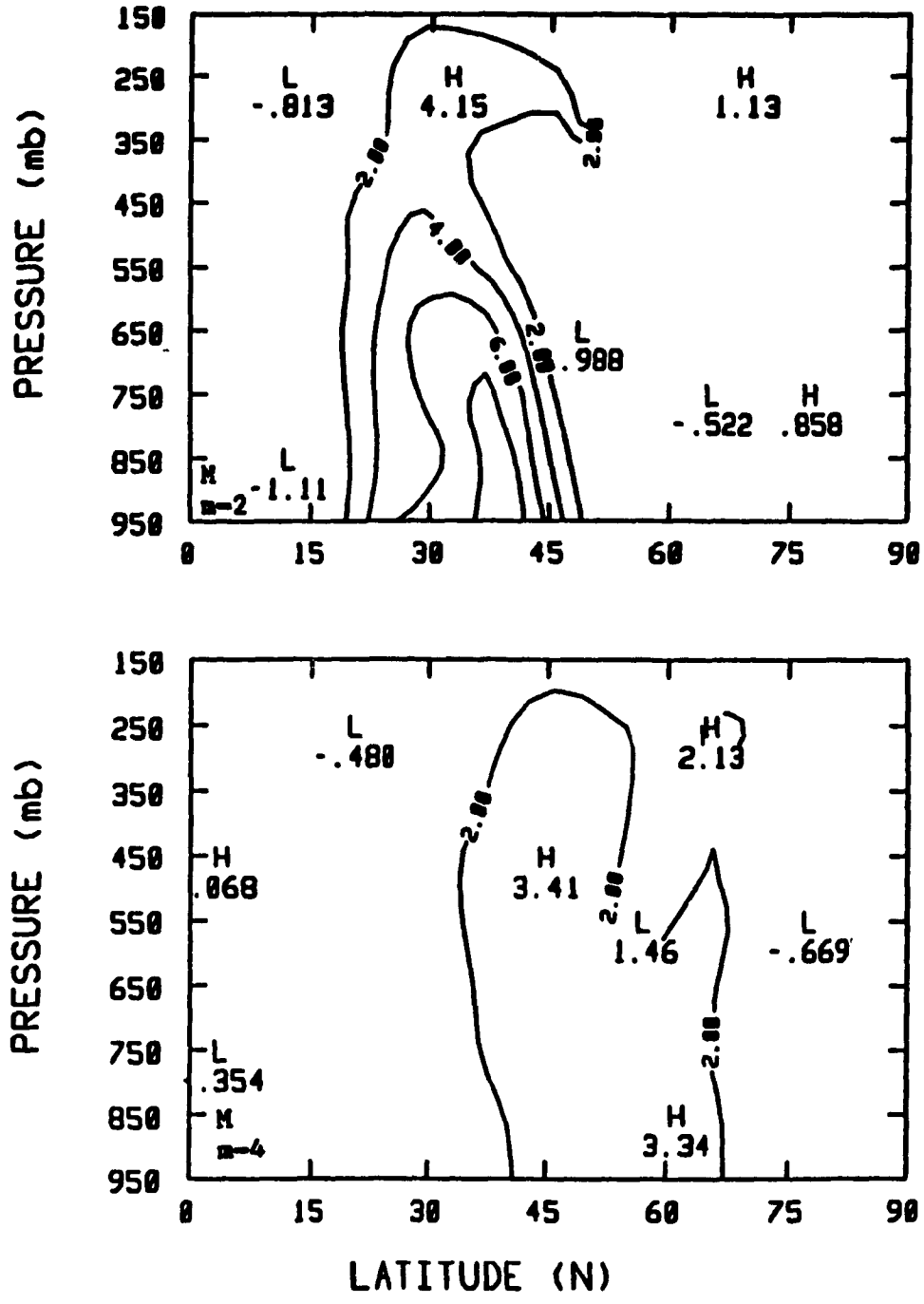

Figure 3.8 As Figure 3.6, but for the contributions of zonal wavenumbers m=2 (up) and m=4 (down) to SE component $[\overline{V^*T^*}]$ for M case. The contour interval is 2 °C m/s, with the zero contour omitted.

troposphere, with comparable contributions from the two zonal wavenumbers m=4, 6 (Figure 3.7). This can be compared to the NM case, where the TE transport is much weaker and is peaked closer to the synoptic scales (m=6, 8; Figure 3.6). The SE heat transport is also much larger in the M case; the transport is dominated by m=2 (Figure 3.8) which is the scale of the topography. The considerable enhancement of the TE heat transport by topography suggests that there is significant wave-wave interaction between the forced SE's and TE's.

3.3 Discussion

In this chapter, we have examined the meridional heat transport by transient and stationary planetary waves. The transports act to reduce the baroclinicity of the observed winter tropospheric zonal flow; the latter is used as the zonal flow forcing. Both the SE and TE heat transports are increased by the presence of topography. A zonal wavenumber decomposition of the SE transport shows that the wavenumber m=2, which corresponds to the scale of the topography, makes the largest contribution. This is consistant with a linear response of the topographically forced SE's. However, the fact that the wavenumber m=4 also makes a contribution to the SE transport suggests that there is some nonlinear interaction among the forced SE's. The TE transport in the NM case is maximum in the zonal scales m=6, 8; this scale is near the radius of deformation of the mid-latitude troposphere. We have examined the linear baroclinic instability of the observed zonally averaged zonal flow used in the zonal flow forcing (Figure 2.2), using the 1-dimensionl height-dependent zonal flow at the latitudes $5^{o}N$, $15^{o}N$, ..., $75^{o}N$. The use of such 1-dimensional slices of the zonal flow for the stability analysis is expected to yield

qualitatively correct results as the former has a relatively broad meridional scale (Fig. 2.2), when compared to the radius of deformation. The maximum linear growth rates occur for the zonal flow at 25°N, which corresponds to the location of maximum thermal wind. The growth rate as a function of zonal (m) and meridional (n) wavenumbers are shown in Figure 3.9. We see that the fastest growing mode is the gravest meridional mode (n=1), and has a zonal scale characteristic of the radius of deformation (m=6-8). The e-folding time is about 2 days. These correspond to well known results of the linear instability of 1-dimensional baroclinic zonal flows. This suggests that the TE transport in the NM case is due to the classic baroclinic instability of a zonal flow as first discussed by Charney (1947) and Eady (1949).

The heat transport properties of the TE's are changed completely by the presence of topography. The zonal scales that account for most of the TE heat transport are now m=4, 6, shifted toward the larger scales from the radius of deformation. The planetary scales (m=2, 4) also make the largest contributions to the SE heat transport in the experiment with topography. The planetary scale TE's and SE's in this case are thus highly baroclinic, transporting a significant amount of heat polewards. Stone (1977) speculated that planetary scale TE's and baroclinic SE's might merely be two different aspects of a single phenomenon - eddies generated by a cooperation between forcing and baroclinic instability. Such eddies would be baroclinic in nature and planetary scale in size, and could contain both TE and SE components. Our results in the M experiment provide evidence that this could be the case. The baroclinic heat-transporting TE's and SE's are principally planetary scale in size, and result from an

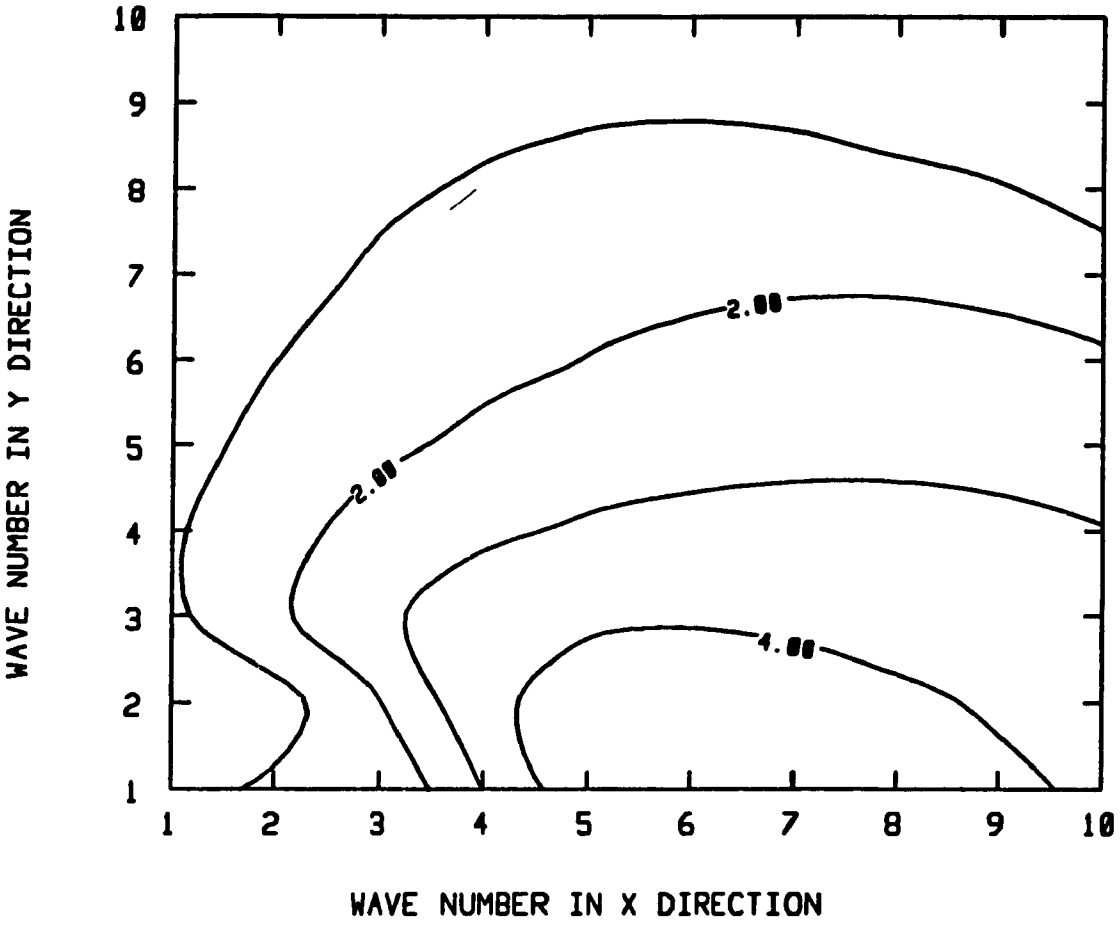

Figure 3.9 Growth rate of fastest growing mode, with the 1-dimensional observed baroclinic zonal flow at 25°N as the basic state. The contour interval is 0.1/day.

interaction between forcing provided by large scale topography and baroclinic instability. The zonally asymmetric topographic forcing creates favoured locations for baroclinically unstable modes to develop, and the resulting planetary wave structure thus has both TE and SE components. This hypothesis has been examined in a series of papers by Lin (1980 a, b), Neelin and Lin (1984) and Lin (1987). Their results, all obtained using linearized theory, show that the baroclinic instability of stationary free and forced zonally asymmetric basic state waves can yield realistic planetary wave structure. There have been other modelling studies which examine the relation between planetary scale TE's and forced SE's; some of these have already been reviewed in Chapter 1. Our results, which focus on the generation of baroclinic planetary waves which transport heat, suggest that nonlinear baroclinic instability in the presence of zonally asymmetric topographic forcing can produce such waves.

CHAPTER 4

Planetary Wave Zonal Heat Transport

4.1 A comparision of observed zonal and meridinoal heat fluxes

There has been much published work on the role of the meridional TE and SE heat fluxes in the large scale atmospheric general circulation. Poleward heat transport by these eddies tends to extract available potential energy (APE) from the mean zonal (Z) flow, resulting in positive conversion of both ZAPE to SEAPE and TEAPE. Peixoto and Oort (1984) provide a review of the energetics of the general circulation. However, there has been relatively little work published on the role of the zonal heat fluxes in the large scale circulation. These fluxes could be significant locally as the general circulation exhibits considerable zonal asymmetries; for example, the time averaged surface termperature structure in winter clearly shows cold continents and warm oceans. Lin (1980a) noted that zonal heat fluxes, as well as meridional heat fluxes, both play important roles in the zonally averaged energetics of modes which result from baroclinic instability of a zonally asymmetric basic state. A motivation for the stability analysis is to examine the relation between forced SE's and planetary scale TE's, as discussed in chapter 1. The zonal heat flux is important because motion in the zonal direction is necessary to release APE associated with the zonal temperature gradient of the basic state. We show in Fig. 4.1 the observed stationary meridional ($\overline{V}^*\overline{T}^*$) and zonal ($\overline{J}^*\overline{T}^*$) heat fluxes in January 1973, computed from National Meteorological Center data. Positive and negative values of the zonal

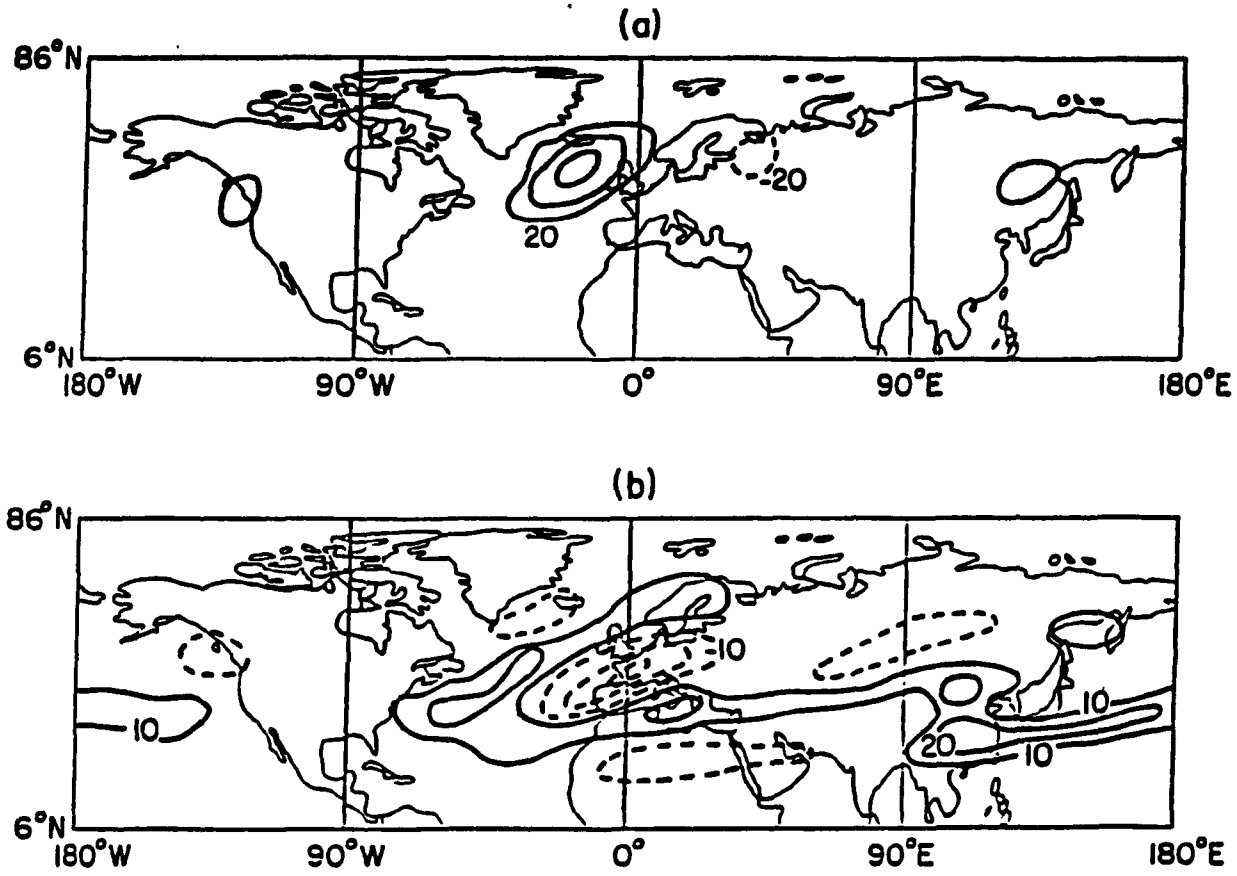

Figure 4.1 Observed stationary meridional and zonal heat flux $\bar{V}^*\bar{T}^*$ (up) and $\bar{U}^*\bar{T}^*$ (down) in January 1973. The contour intervals are 20×10^{17} cal/day (up) and 10×10^{17} cal/day (down).

fluxes are present; this is in contrast to the meridional flux, where positive values corresponding to poleward heat transport, are more dominant. However, the magnitudes of both fluxes are comparable. Lin (1987) noted that this might be associated with the fact that the storm tracks, which are favoured regions of eddy development off the east coast of continents, are oriented parallel to the ocean/continent margin.

The transient meridional ($\overline{V'T'}$) and zonal ($\overline{U'T'}$) heat fluxes are shown in Fig. 4.2. The meridional flux shows a planetary scale zonal structure, with prominent maxima off the east coast of continents, at the locations of the storm tracks. The zonal fluxes are smaller in magnitude and are less organized in structure, but they could be large locally. The total meridional and zonal heat fluxes, consisting of the sums of the stationary and transient contributions, are shown in Fig. 4.3. The meridional flux pattern remains similar to both the stationary and transient components, as the latter two resemble each other. The magnitude is , of course, larger than that of either component. The total zonal flux is dominated by the stationary contribution. It is clear that both the total meridional and zonal heat fluxes are planetary scale in structure and are comparable in magnitudes.

The eddy heat fluxes play an important role in the energetis of the general circulation. We have already mentioned the conversion of ZAPE to SEAPE and TEAPE. There have been many published studies on the nature of these conversions. However, the conversion between SEAPE and TEAPE has only been examined in two published studies (Holopainen, 1970; Lau and Oort, 1982). This conversion can be represented mathematically as

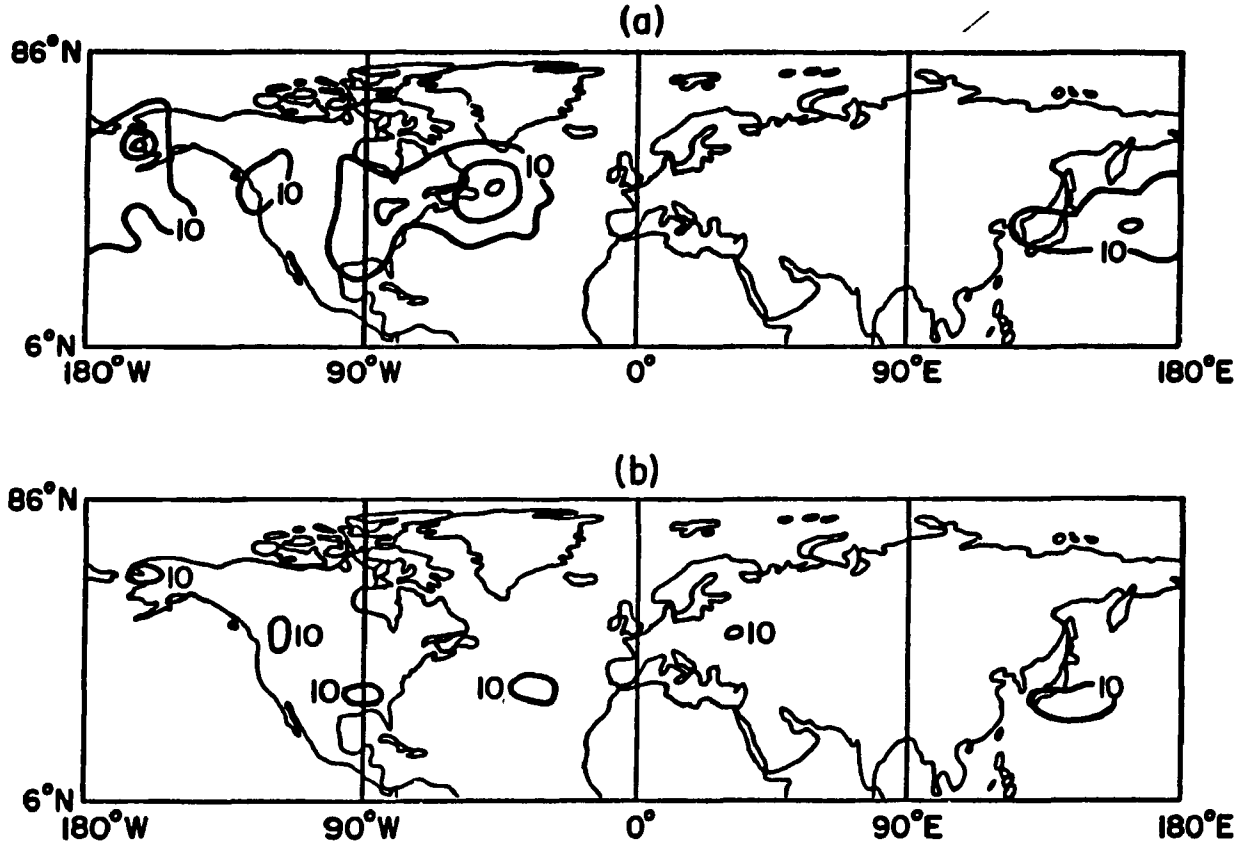

Figure 4.2 As Fig. 4.1 but for the transient meridional $\overline{V'T'}$ (up) and zonal $\overline{U'T'}$ (down) heat fluxes. The contour interval is 10×10^{17} cal/day.

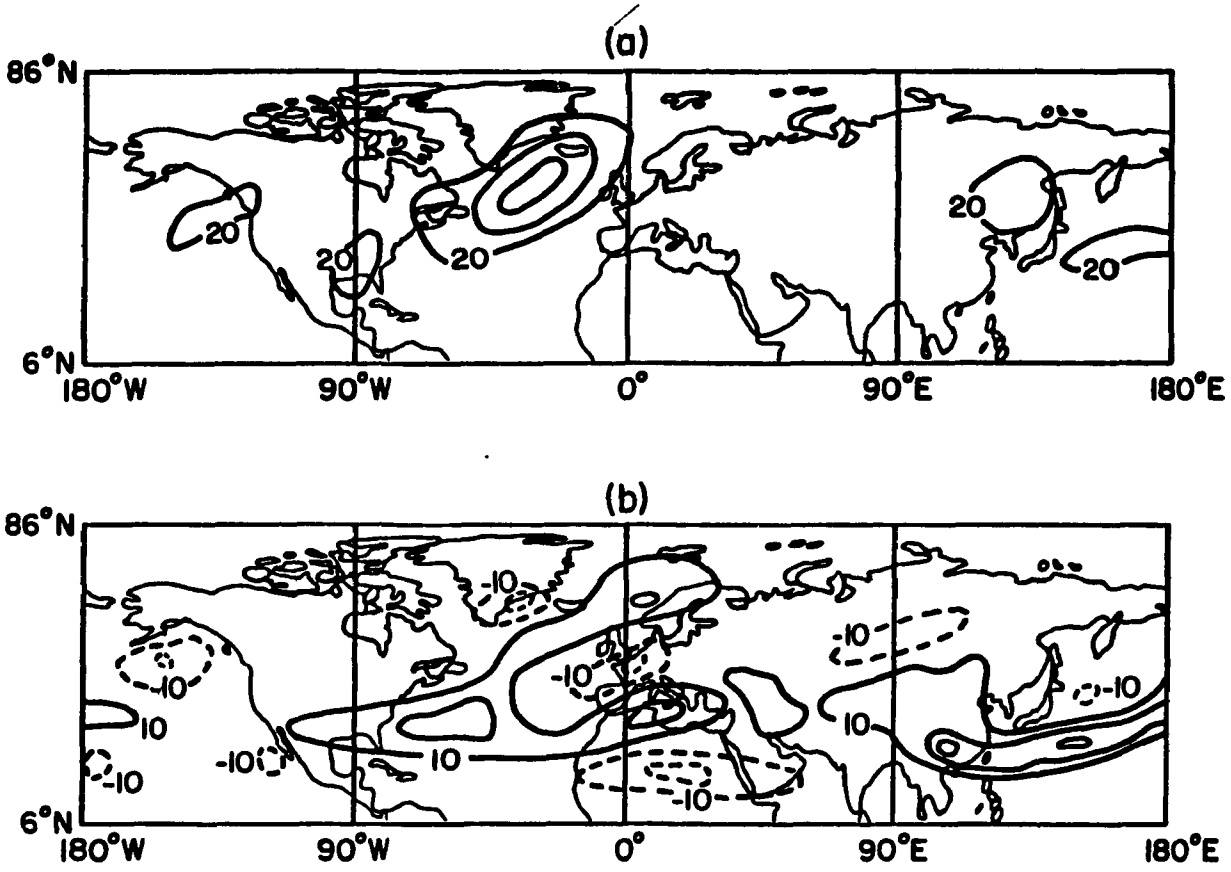

Figure 4.3 As Fig. 4.1 but for the total meridional $\overline{\overline{v}'\overline{T}'} + \overline{v}^*\overline{T}^*$ (up) and zonal $\overline{\overline{U}'\overline{T}'} + \overline{U}^*\overline{T}^*$ (down) heat fluxes. The contour intervals are 20×10^{17} cal/day (up) and 10×10^{17} cal/day (down).

$$C(SEAPE, TEAPE) = -C_p \int \gamma \left(\frac{\overline{U'T'}^*}{a \cos\phi} \frac{\partial \overline{T}^*}{\partial \lambda} + \frac{\overline{V'T'}^*}{a} \frac{\partial \overline{T}^*}{\partial \phi} \right) dm \qquad (4.1)$$

where γ is the stability factor

$$\gamma = -\frac{\theta}{T} \frac{R}{C_p P} \frac{\partial p}{\partial \bar{\theta}}$$

with ~ denoting a horizontal average. The integration is over the mass of the atmosphere, with dm being the mass element. Physically, the conversion is due to the zonally asymmetric component of the transient zonal and meridional heat fluxes, transporting heat toward or away from different regions of the zonally asymmetric stationary temperature field. The conversion is positive if there is an overall tendency to transport heat toward cooler regions, and away from warmer regins, on the same latitude circle. This means the transient heat fluxes are acting to reduce the zonal asymmetries of the stationary eddy temperature field, i.e., reducing SEAPE. Lau and Oort (1982) evaluated various transient eddy statistics using two sets of observed circulation statistics, prepared at GFDL (Geophysical Fluid Dynamics Laboratary) and at NMC (National Meteorological Center). They noted that the heat flux vectors in both data sets showed a distinct tendency to be directed toward lower temperatures. The eddy heat transports converge over northeast Canada and eastern Siberia, which are colder than other regions in the same zonal belt; the transports diverge over the relatively warm oceans. This means the TE's act to destroy the departures from zonal symmetry of the temperature field, resulting in a positive conversion of SEAPE to TEAPE. Boer and Sargent (1985) examined the vertically integrated global energy budget using FGGE III-b data. They found that the nonzonal component of the transient energy flux is dominated by temperature terms since the transient transport of potential energy is

small. The transient fluxes of energy from the Gulf Stream and storm track region of the Atlantic is directed northward and westward toward cold continent in January, in agreement with the results of Lau and Oort. We next examine the conversion C(SEAPE,TEAPE) in our model results.

4.2 The energy conversion C(SEAPE,TEAPE)

Our model is formulated on a mid-latitude β-plane. The expression (4.1) for the conversion C(SEAPE, TEAPE), written for spherical geometry, then becomes

$$C(SEAPE,TEAPE) = -C_p \int \gamma \left(\overline{U'T'}^* \frac{\partial \overline{T}^*}{\partial x} + \overline{V'T'}^* \frac{\partial \overline{T}^*}{\partial y}\right) dm \qquad (4.2)$$

with Carterian coordinates x, y replacing spherical coordinates λ, ϕ respectively. We have examined latitude-pressure sections of the zonal average of the integrand of (4.2); more specifically, the zonally averaged quantity

$$C(SEAPE,TEAPE) \sim -C_p \gamma \left[\overline{U'T'}^* \frac{\partial \overline{T}^*}{\partial x} + \overline{V'T'}^* \frac{\partial \overline{T}^*}{\partial y} \right] \qquad (4.3)$$

is examined as a sum of contributions from different zonal wavenumbers in the TE horizontal heat transports ($\overline{U'T'}^*, \overline{V'T'}^*$), and the SE temperature field ($\overline{T}^*$). This is of great interest as both the heat flux and SE temperature field are expected to be dominated by the planetary scale, due to the zonal asymmetries introduced by the surface topography. This is indeed the case for the M experiment. In the NM case, the conversion shows no organized structure on the latitude-pressure plane, as there are no favoured locations for eddy development. In the M case, the conversion term (4.3) is dominated by zonal wavenumber m=2 in both the horizontal heat flux and SE temperature field; the contributions from the other zonal

wavenumbers are all small. The corresponding latitude-pressure cross section is shown in Fig. 4.4. We see a prominent maximum at around 30°N in the upper troposphere, indicative of strong conversion of SEAPE to TEAPE in these regins. As disscussed earlier, this conversion results from eddy heat transports down the local time averaged temperature gradient. This mechanism is examined more closely in Fig. 4.5, where we show the TE heat flux vector $\underline{F} = (\overline{U'T'}^*, \overline{V'T'}^*)$ superposed on the SE temperature field $\overline{T}^*$ at 250mb. From (4.3), we see that a strong conversion of SEAPE to TEAPE is associated with the heat flux $\underline{F}$ being almost perpendicular to the $\overline{T}^*$ field, directed from high to low temperatures. In Fig. 4.5, this is found near 30°N, at a longitude of about 120° at the lee of the topography. There is a strong heat flux directed from the high in the $\overline{T}^*$ field to the low to the east and north. Equivalently, there is TE heat flux divergence over the $\overline{T}^*$ high, and convergence near the $\overline{T}^*$ low. This reduces the temperature gradient of the SE temperature field, resulting in a conversion of SEAPE to TEAPE.

When integrated over the model domain, (4.3) gives the total conversion C(SEAPE,TEAPE). We have also evaluated the total conversions of ZAPE to SEAPE and of ZAPE to TEAPE; other non-baroclinic conversions involving these energy forms are not considered here.

$$C(ZAPE,SEAPE) = - C_p \int \gamma \left(\overline{V}^* \overline{T}^* \frac{\partial [\overline{T}]}{\partial y} \right) dm$$

$$C(ZAPE,TEAPE) = - C_p \int \gamma \left(\overline{V'T'} \frac{\partial [\overline{T}]}{\partial y} \right) dm$$

The total energy conversion among ZAPE, SEAPE and TEAPE are shown in Fig. 4.6, for both the NM and M experiments. In the former case, the SE's

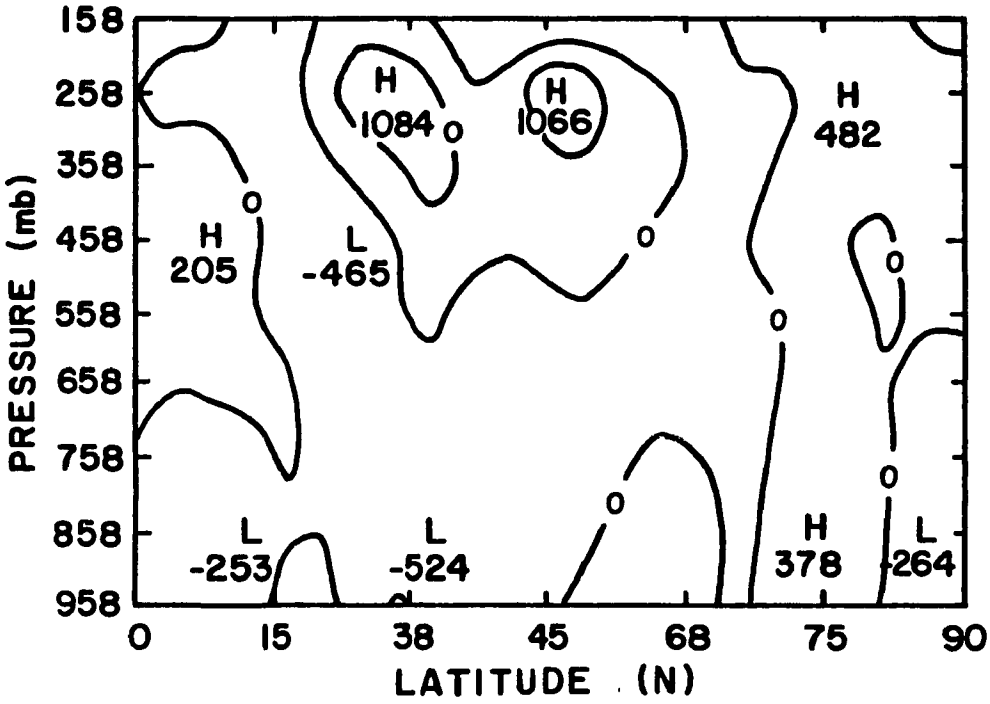

Figure 4.4 The latitude-pressure section of the contribution by zonal wavenumber m=2 to conyersion term in eq. (4.3) for M case. The contour interval is 500 j/s m^2.

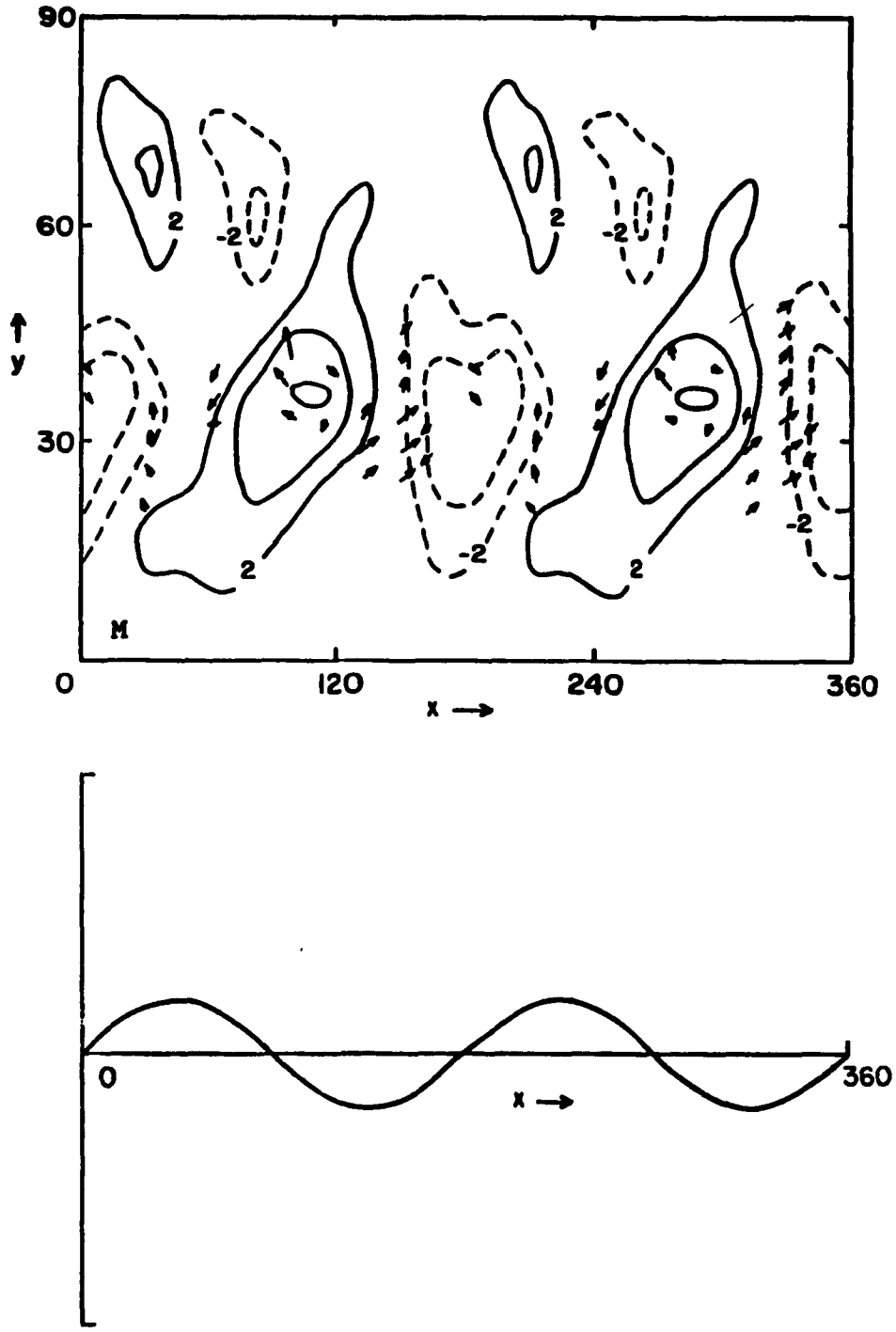

Figure 4.5 The upper panel shows the zonal-meridional (x-y) section at 250mb for the M case TE heat flux vector ($\overline{U'T'}^*, \overline{V'T'}^*$) superposed on the SE temperature field $\overline{T}^*$. The largeset vector has an amplitude of 58°C m/s. The contour interval of the $\overline{T}^*$ field is 2°C with the zero contour omitted. The bottom panel shows the zonal distribution of the surface topography used in the M experiment.

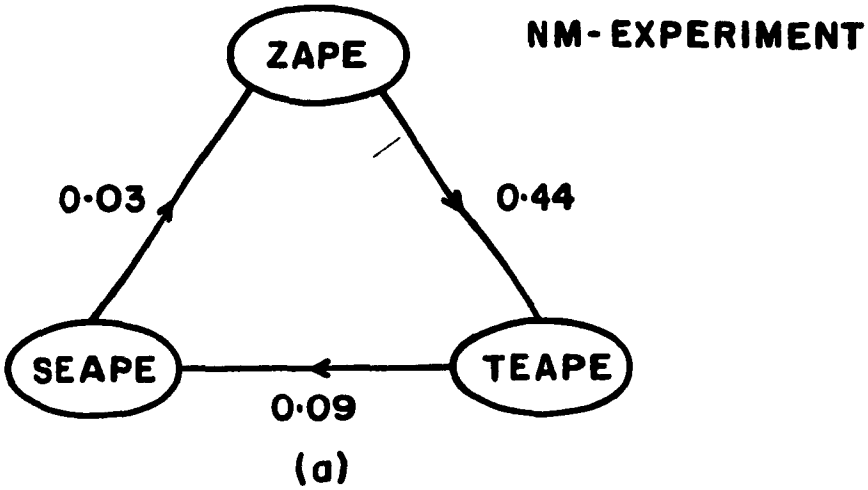

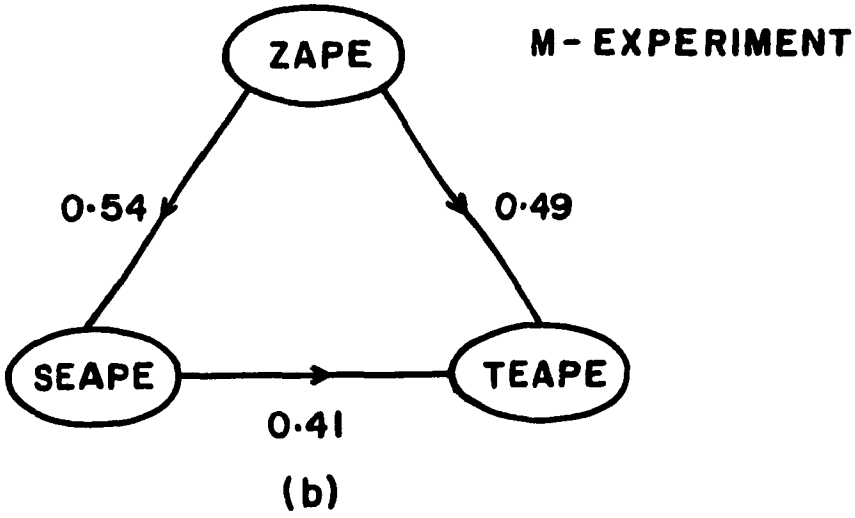

Figure 4.6 Energy conversion among ZAPE, SEAPE and TEAPE for NM (up) and M (down) experiments. The unit is 10^{13} j/s.

are weak and are ineffective at extracting ZAPE; the dominant conversion is thus C(ZAPE,TEAPE), which is associated with TE meridional heat flux reducing the mean meridional temperature gradient. The energetics is changed completely with the presence of surface topography. The TE's are still maintained by the baroclinic instability of the zonal flow, but ZAPE also maintains the SE's via the SE meridional heat flux. The SE's in turn help to maintain the TE's via the baroclinic conversion C(SEAPE,TEAPE) examined earlier. Moreover, all these conversions C(ZAPE,SEAPE), C(ZAPE,TEAPE) and C(SEAPE,TEAPE) are of comparable magnitudes. This suggests that zonal asymmetries due to surface topography together with baroclinic instability play a fundamental role in the maintainence of planetary waves.

4.3 Discussion

We have examined the zonal heat fluxes of planetary waves in this chapter. Observational results show that the zonal and meridional fluxes are comparable in magnitude and have planetary scale zonal structures. Diagnostic studies by Lau and Oort (1982) show that TE heat fluxes act to destroy the departures from zonal symmetry of the time averaged temperature field, thus resulting in a positive conversion C(SEAPE,TEAPE). This aspect of the role of the TE heat flux is captured in our M experiment. As we saw in Chapter 3, the presence of surface topography led to a significant increase of the TE meridional heat flux, leading to an enhanced conversion of SEAPE to TEAPE. However, this enhancement is also due to an increased TE zonal heat flux, as seen from the west-east orientation of the TE heat flux vector in Fig. 4.5. Moreover, the zonal wavenumber in both the TE horizontal heat flux and $\overline{T}^*$ field giving the enhanced conversion is m=2, in

the planetary scales. This is consistant with the idea that planetary scale TE's which transport heat are due to baroclinic instability of the SE field forced by zonal asymmetries (Stone, 1977). In our model, the zonally asymmetric forcing is provided by surface topography at zonal wavenumber m=2; effects of diabatic forcing due to land/sea temperature differences are not considered. This might be the reason why the conversion C(SEAPE,TEAPE) maximum is located in the upper troposphere (Fig. 4.4) instead of at the surface. Diagnostic studies using observational data show that the correlation between the SE temperature field $\overline{T}^*$ and the TE heat flux divergence is strongest in the lower troposphere and decreases rapidly with height (Lau and Wallace, 1979; Lau and Oort, 1982). This means that the conversion from SEAPE to TEAPE should be maximum in the lower troposphere. Inclusion of surface diabatic forcing in our model is expected to lower the maximum presently found in the upper troposphere.

Lau and Oort (1982) also calculated the baroclinic conversions of Fig. 4.6 using the GFDL and NMC observational data sets. Due to the simplified nature of our model, such as the lack of spherical geometry and surface diabatic forcing, detailed comparision with observational results is not possible. In Fig. 4.7, we show a comparision of the three baroclinic conversions, normalized by the conversion C(ZAPE,TEAPE), between our results from the M experiment and those from the GFDL and NMC datasets, as given in Lau and Oort. The normalized conversions in the GFDL and NMC results are very close, although the conversion C(ZAPE,TEAPE) itself differs between the two, 1.7×10^5 j/m^2 for GFDL, and 2.2×10^5 j/m^2 for NMC (Lau and Oort, 1982). The importance of the baroclinic conversions ZAPE → TEAPE, ZAPE → SEAPE → TEAPE are clearly shown in these observational

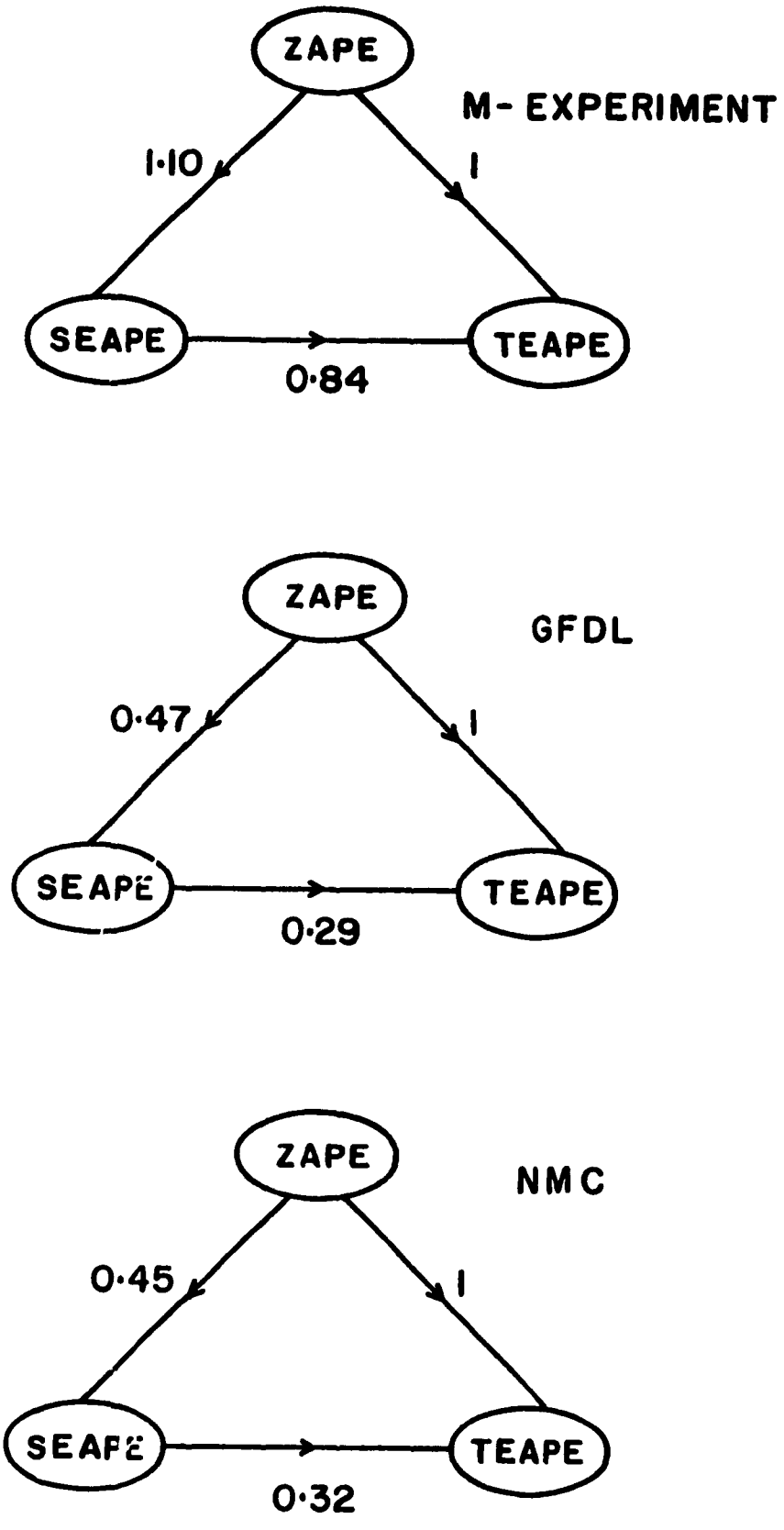

Figure 4.7 Normalized energy conversions among ZAPE, SEAPE and TEAPE for the M experiment, GFDL and NMC data sets. Values for the latter two cases are adapted from Lau and Oort (1982).

results. Our M-experiment shows the various conversion as having comparable values; this means the conversions ZAPE → SEAPE → TEAPE are overestimated when compared to observational results. However, it is clear that the baroclinic conversion C(SEAPE,TEAPE) due to zonal and meridional heat fluxes reducing the SE temperature field, is captured in the model with surface topography acting as the zonally asymmetric forcing.

CHAPTER 5

Conclusions

We have used a 10-level nonlinear quasi-geostrophic β-plane model to examine the heat transport of planetary waves. The motivation for this study is to examine the mechanistic role of surface topography in generating baroclinic planetary waves. The dependance of the eddy statistics on zonal wavenumber, and the interaction between TE's and SE's via the baroclinic conversion of SEAPE to TEAPE, are of particular interest.

The presence of both nonlinearity and surface topography as zonally asymmetric forcing leads to an enhanced TE meridional heat transport, as well as SE heat transport. In the absence of surface topography, the TE heat transport is dominated by zonal scales near the radius of deformation, while the SE transport is negligible. The former result is consistent with the theory of classic baroclinic instability of zonal flows; the latter result is expected as there are no preferred regions of development in the absence of zonally asymmetric forcing. The presence of surface topography shifts the zonal wavenumber peak of the eddy heat transport from the synoptic scales to the larger planetary scales. This is consistent with the results of Lin (1980b), who showed that the zonal scale selected by linear baroclinic instability of zonally asymmetric flows lies between the radius of deformation and the scale of the asymmetric forcing. Our results demonstrate that this is also valid in the nonlinear regime.

A particularly relevant aspect of the energetics of the planetary waves is the conversion of SEAPE to TEAPE. This is accomplished by the transient eddy heat flux directed down the local temperature gradient. The eddy heat flux has both a meridional and zonal component. This is necessary as the local temperature contours are not zonal. We conclude from NMC observational data that the total zonal heat flux can be locally as large as the meridional flux. The model heat flux demonstrates clearly the dissipative role of TE's on the zonally asymmetric component of the time mean temperature field.

A limitation of the model is the lack of spherical geometry and the relativelly low horizontal spatial resolution. Moura and Stone (1976) examined the baroclinic instability of simple 2-dimensional zonal wind shear profiles on a sphere, using a linear 2-layer quasi-geostrophic model They found that the structure of the most unstable modes are qualitatively similar to those on a β-plane. For example, the unstable waves far from neutral stability have amplitudes which show a quasi-Gaussian behaviour with latitude on both the sphere and the β-plane. As to the low horizontal resolution used, we note that O'Brien and Branscome (1989) have produced a "minimal" model of the atmospheric general circulation using a two-layer quasi-geostrophic model with much lower resolution – 3 waves in both the zonal and meridional directions. We have not tuned the model parameters to best reproduce aspects of the observed general circulation. Our main goal here is to examine the mechanistic role of surface topography as a zonally asymmetric forcing, and baroclinic instability in generating baroclinic planetary waves. Our results indicate that forcing and instability can indeed work to produce planetary waves with realistic heat transport

properties, as first suggested by Stone (1977). It would thus be of great interest to examine this mechanism using more realistic models.

REFERENCE

Asselin, R., 1972: Frequency filter for time integrations, Mon.Weather Rev. 100, 487-490.

Boer, G.J. and Sargent, N.E., 1985: Vertically integrated budget of mass and energy for the globe. J.Atmos.Sci. 42, 1592-1613.

Charney, J.G., 1947: The dynamics of long waves in a baroclinic westerly current. J.Meteor. 4, 135-163.

Eady, E.J., 1949: Long waves and cyclone waves. Tellus 1, 33-52.

Frederiksen, J.S., 1978: Instability of planetary waves and zonal flows in two-layer models on a sphere. Quart.J.Roy.Meteor.Soc. 104, 841–872.

———, 1980: Zonal and meridional variations of eddy fluxes induced by long planetary waves, Quart.J.Roy.Meteor.Soc. 106, 63-84.

———, 1981: Disturbances and eddy fluxes in southern hemisphere flows: Linear theory. J.Atmos.Sci. 38, 673–689.

———, 1982: A unified three-dimensional instability theory of the onset of blocking and cyclogenesis, J.Atmos.Sci., 40, 2593-2609.

———, 1983a: Disturbances and eddy fluxes in Northern Hemisphere flow: Instability of three-dimensional January and July flows, J.Atmos. Sci. 40, 836-855.

———, 1983b: A unified three-dimensional instability theory of the onset of blocking and cyclogenesis. II: teleconnection patterns, J.Atmos. Sci. 40, 2593-2609.

Gall, R., 1976: Structural changes of growing baroclinic waves. J.Atmos. Sci. 33, 374-390.

Green, J.S.A., 1970: Transfer properties of large-scale eddies and the general circulation of the atmosphere. Quart.J.Roy.Meteor.Soc. 96, 157–185.

Grotjahn, R., 1984: Baroclinic instability in a long wave environment. Part I: Review, Quart.J.Roy.Meteor.Soc. 110, 663-668.

Haltiner, G.J. and R.T. Williams, 1980: Numerical Prediction and Dynamic Meteorology, (2nd edition) John Wiley and Sons, New York, 477 pp.

Holopainen, E.O., 1970: An observational study of the energy balance of the stationary disturbances in the atmosphere, Quart.J.Roy.Meteor.Soc. 96 626-644.

Kao S.K. and J.F. Sagendorf, 1970: The large-scale meridional transport of sensible heat in wavenumber-frequency space, Tellus 22, 172-185.

Kirkwood, E. and J. Derome, 1977: Some effects of the upper boundary condition and vertical resolution on modelling forced stationary planetary waves, Mon.Wea.Rev. 105, 1239-1251.

Lau, N.C., 1979: The observed structure of tropospheric stationary waves and the local balances of vorticity and heat, J.Atmos.Sci. 36, 996 -1016.

Lau, N.C. and J.M. Wallace, 1979: On the distribution of horizontal transport by transient eddies in the Northern Hemisphere wintertime circulation, J.Atmos.Sci. 36, 1844-1861.

Lau, N.C. and A.H. Oort, 1982: A comparative study of observed Northern Hemisphere circulation statistics based on GFDL and NMC analyses. Part II: Transient eddy statistics and the energy cycle, Mon.Wea. Rev. 110, 889-906.

Lin, C.A., 1980a: Eddy heat fluxes and stability of planetary waves. Part I, J.Atmos.Sci. 37, 2353-2372.

———, 1980b: Eddy heat fluxes and stability of planetary waves. Part II, J.Atmos.Sci. 37, 2373-2380.

———, 1987: Instability of planetary waves in a high vertical resolution model, Geophy.Astrophy. Fluid Dyn. 39, 227–259.

Lin, C.A. and A. Chan, 1988: Baroclinic instability and the summer Southern Hemisphere wavenumber 5 circulation, Geophy.Astrophy.Fluid Dyn. (in press).

Lindzen, R.S., E.S. Batten and J.W. Kim, 1968: Oscillations in atmospheres with tops, Mon.Wea.Rev. 96, 133–140.

Lorenz, E.N., 1963: The mechanics of vacillation, J.Atmos.Sci. 20, 448-464

Mitchell, H.L., 1982: Resonance of stationary waves in a model atmosphere, Ph.D. thesis, McGill University, 220 pp. [available as Report 125, Department of Meteorology, McGill University].

Mitchell, H.L. and J. Derome, 1983: Blocking-like solutions of the potential vorticity equation: their stability at equilibrium and

growth at resonance. J.Atmos.Sci. 40, 2522-2536.

———, 1985: Resonance of topographically forced waves in a quasi-geostrophic model, J.Atmos.Sci. 42, 1653-1666.

Moura A.D. and P.H. Stone, 1976: The effects of spherical geometry on baroclinic instability, J.Atmos.Sci. 33, 602—616.

Neelin, J.D. and C.A. Lin, 1984: Baroclinic generation of planetary transient and stationary waves from forced stationary waves, J. Geophys.Res. 89, D5, 7202-7214.

O'Brien E. and L.E. Branscome L.E., 1988: Modes of variability in a low-order two-level model, Tellus, 40, 358-374.

——— and ———, 1989: Minimal modeling of the extratropical general circulation Tellus (in press).

Oort, A.H. and E.M. Rasmusson, 1971: Atmospheric circulation statistics, NOAA Professional Paper 5 (U.S. GPO Washington D.C.).

Peixoto, J.P. and A.H. Oort, 1984: Physics of climate, Rev.Mod.Phy. 56, 365—430.

Robert, A.J., 1966: The integration of a low order spectral form of the primitive meteorological equations, J.Meteor.Soc.Japan 44, 237–245.

Sasamori, T. and C.E. Youngblut, 1981: The nonlinear effects of transient and stationary eddies on the winter mean circulation. Part II: The stability of stationary waves, J.Atmos.Sci. 38, 87-96.

Simmons, A.J. and B.J. Hoskins, 1977: Baroclinic instability on the sphere: solution with a more realistic tropopause, J.Atmos.Sci. 34, 581–588.

Simmons, A.J., J.M. Wallace and G.W. Branstator, 1983: Barotropic wave propagation and instability and atmospheric teleconnection patterns. J.Atmos.Sci. 40, 1363-1392.

Stone, P.H., 1977: Generation of atmospheric eddies, Investigations of the Synoptic Variablity of the Ocean, V.M. Kamenkovich and P.B. Rhines, Eds., Acad. Sci. USSR, Sevastopol, 400-421.